Article
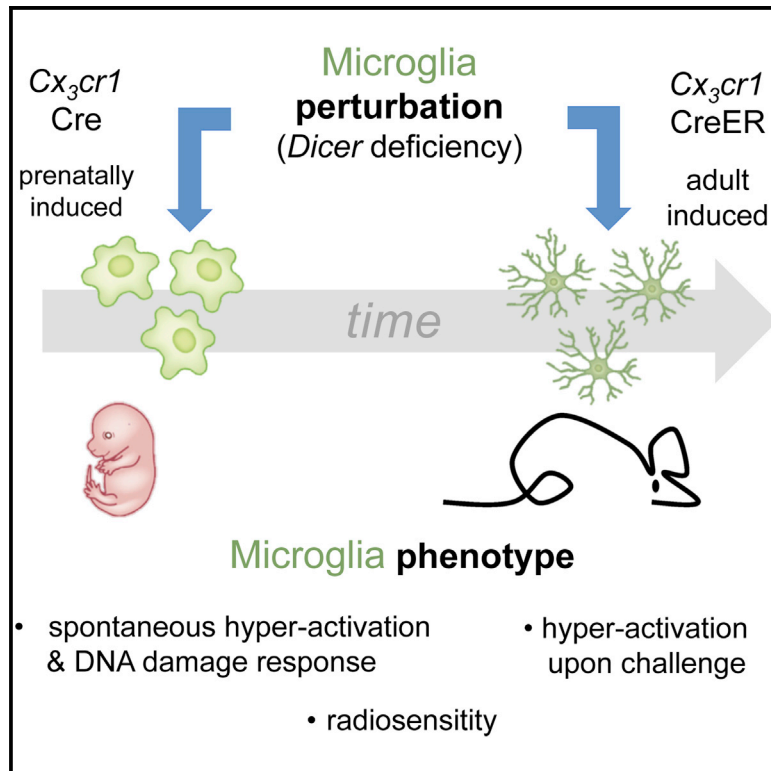
Dicer Deficiency Differentially Impacts Microglia of the Developing and Adult Brain

Graphical Abstract

Authors

Diana Varol, Alexander Mildner, Thomas Blank, ..., Nicola Maggio, Marco Prinz, Steffen Jung

Correspondence

s.jung@weizmann.ac.il

In Brief

Microglia of developing and adult brain differ in activation state and function. Here, Varol and colleagues ablated microglial Dicer expression at distinct times. Adult microglia tolerated the perturbation but became hyper-responsive to challenge compromising hippocampus functions. *Dicer* and microRNA absence during development caused spontaneous microglia activation and impaired genome integrity.

Highlights

- miRNAs curb activation of adult microglia after challenge

- Adult microglia hyper-activation impairs hippocampal neuronal functions

- Dicer-deficient microglia proliferating in developing brain accumulate DNA damage

- Microglia of the developing and adult brain are functionally distinct

CrossMark

CellPress

Dicer Deficiency Differentially Impacts Microglia of the Developing and Adult Brain

Diana Varol,[1] Alexander Mildner,[1] Thomas Blank,[2] Anat Shemer,[1] Neta Barashi,[1] Simon Yona,[1] Eyal David,[1] Sigalit Boura-Halfon,[1] Yifat Segal-Hayoun,[1] Louise Chappell-Maor,[1] Hadas Keren-Shaul,[1] Dena Leshkowitz,[3] Eran Hornstein,[4] Martin Fuhrmann,[5] Ido Amit,[1] Nicola Maggio,[6] Marco Prinz,[2,7] and Steffen Jung[1,8,*]

[1]Department of Immunology, The Weizmann Institute of Science, 76100 Rehovot, Israel
[2]Institute of Neuropathology, Medical Faculty, University of Freiburg, 79106 Freiburg, Germany
[3]Life Sciences Core Facilities, The Weizmann Institute of Science, 76100 Rehovot, Israel
[4]Department of Molecular Genetics, The Weizmann Institute of Science, 76100 Rehovot, Israel
[5]Neuroimmunology and Imaging, German Center for Neurodegenerative Diseases (DZNE), 53105 Bonn, Germany
[6]Department of Neurology, The Chaim Sheba Medical Center, Sackler Faculty of Medicine and Sagol School of Neuroscience, Tel Aviv University, 5262 Tel Aviv, Israel
[7]BIOSS Centre for Biological Signalling Studies, University of Freiburg, 79106 Freiburg, Germany
[8]Lead Contact
*Correspondence: s.jung@weizmann.ac.il
http://dx.doi.org/10.1016/j.immuni.2017.05.003

SUMMARY

Microglia seed the embryonic neuro-epithelium, expand and actively sculpt neuronal circuits in the developing central nervous system, but eventually adopt relative quiescence and ramified morphology in the adult. Here, we probed the impact of post-transcriptional control by microRNAs (miRNAs) on microglial performance during development and adulthood by generating mice lacking microglial *Dicer* expression at these distinct stages. Conditional *Dicer* ablation in adult microglia revealed that miRNAs were required to limit microglial responses to challenge. After peripheral endotoxin exposure, *Dicer*-deficient microglia expressed more pro-inflammatory cytokines than wild-type microglia and thereby compromised hippocampal neuronal functions. In contrast, prenatal *Dicer* ablation resulted in spontaneous microglia activation and revealed a role for Dicer in DNA repair and preservation of genome integrity. Accordingly, *Dicer* deficiency rendered otherwise radio-resistant microglia sensitive to gamma irradiation. Collectively, the differential impact of the Dicer ablation on microglia of the developing and adult brain highlights the changes these cells undergo with time.

INTRODUCTION

Tissue macrophage compartments evolve locally and independently from each other alongside their organ microenvironment (Amit et al., 2016; Ginhoux and Guilliams, 2016). Macrophages are hence intimately associated with their immediate surroundings and acquire, beyond their established generic function as immune sentinels, activities tailored to assist local tissue needs (Varol et al., 2015). Microglia are yolk sac-derived macrophages residing in brain and spinal cord, where they interact with neurons and other glial cells, constantly probing the parenchyma with dynamic extensions (Davalos et al., 2005; Nimmerjahn et al., 2005). Microglia actively contribute to synaptic pruning, and microglial interactions with synaptic elements are affected by neuronal activity. This notion is supported by sustained neuronal phenotypes and functional deficits in neuronal connectivity in mice harboring microglia mutant for complement or CX_3CR1 chemokine receptors (Paolicelli et al., 2011; Schafer et al., 2012). Contributions of microglia to physiological brain function are further underlined by neuropsychiatric or neurologic disorders linked to microglial dysfunctions (Prinz and Priller, 2014). This includes *CSF1R* mutation-associated hereditary diffuse leuko-encephalopathy with spheroids (HDLS) (Rademakers et al., 2011), as well as fronto-temporal dementia and Alzheimer's disease linked to genetic *TREM2* variations (Guerreiro and Hardy, 2013; Poliani et al., 2015; Wang et al., 2015).

Differentiation and tissue-specific activation of macrophages require precise regulation of gene expression that is governed by epigenetic mechanisms, such as DNA methylation, histone modifications, and chromatin structure (Amit et al., 2016). Expression signatures are further subject to post-transcriptional and post-translational regulation. A major established post-transcriptional filter comprises regulation by microRNAs (miRNAs), a family of small non-coding RNAs (ncRNAs) that shape gene expression under physiological and pathophysiological conditions (Bartel, 2009). miRNAs are generated from hairpin structured pre-miRNA transcripts that are processed in the cytoplasm by the ribonuclease type III Dicer1 (Dicer) (Bernstein et al., 2003). Once mature, Dicer loads the ~22 nucleotide-long single-stranded miRNAs onto the RNA-induced silencing complex (RISC) that targets mRNAs, based on sequence complementarity between their 3′ untranslated region (UTR) and the respective miRNAs (Guo et al., 2010).

Here we investigated the role of miRNA-based post-transcriptional regulation for the maintenance of microglia identity and function. Specifically, we used constitutive or inducible *Cx3cr1* promoter-driven Cre recombinase combined with conditional *Dicer* alleles to generate animals whose microglia lack Dicer
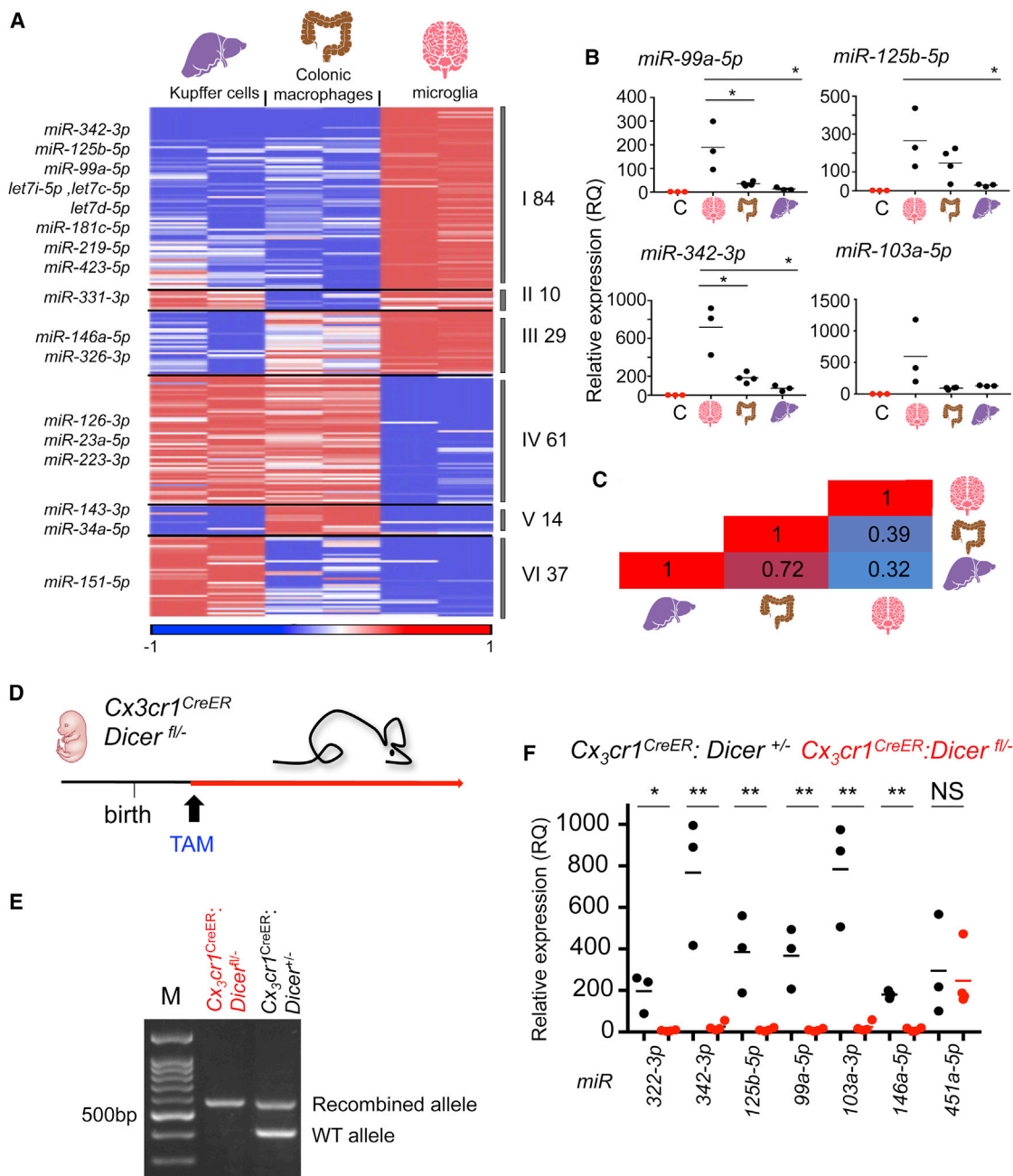
Figure 1. Microglia Display a Distinct MicroRNA Profile as Compared to Other Tissue Macrophages

(A) Heatmap of miRNA expression measured by Agilent microarray of sorted microglia, liver (KCs), and colon macrophages from 6-week-old mice. Shown are miRNAs exhibiting >2 statistically significant fold change (measured by ANOVA) between any two distinct populations (235 miRNAs). Intensity values were log-transformed, normalized, and centered, and genes were clustered by a Pearson correlation test, number of partition clusters was set to six. Data are from one experiment, including two replicates per cell type; each replicate represents a pool of six mice.

(B) qRT-PCR analysis for expression of selected miRNAs in microglia, colonic macrophages, and Kupffer cells. Data are from one experiment including negative control microglia (labeled "C") isolated from brains of TAM-treated $Cx3cr1^{CreER}:Dicer^{fl/-}$ mice (see D–F) (n = 3), microglia (n = 3), colon MF (n = 4), and KCs (n = 3), statistically analyzed with one-way ANOVA for multiple comparisons (*p < 0.05).

(C) Correlation matrix with Pearson correlation coefficient performed for all miRNAs expressed above background and displaying >2 statistically significant fold change between any two populations displayed in (A).

(D) Scheme illustrating conditional TAM-induced mutagenesis using $Cx3cr1^{CreER}:Dicer^{fl/-}$ mice.

(E) Genomic PCR analysis of sorted brain microglia of $Cx3cr1^{CreER}:Dicer^{fl/-}$ mice and controls, 6 weeks after TAM treatment given at 4 weeks of age. Data are representative of three independent experiments, including $Cx3cr1^{CreER}:Dicer^{fl/-}$ (n = 7) and $Cx3cr1^{CreER}:Dicer^{+/-}$ (n = 6) mice.

(legend continued on next page)

and as a consequence, miRNAs and other Dicer-dependent small non-coding RNAs.

We showed that the absence of Dicer, when introduced postnatally, led to a reduction of microglia abundance but was largely compatible with microglial steady-state performance. However, miRNAs were required to curb microglia activation after peripheral endotoxin encounter, when *Dicer*-deficient microglia displayed increased expression of pro-inflammatory cytokines resulting in impairment of hippocampal synaptic transmission. In contrast, prenatal *Dicer* ablation caused spontaneous microglia activation and an accumulation of DNA damage. Corroborating the role of Dicer in DNA repair, *Dicer*-deficient microglia of both developing and adult brain were rendered radio-sensitive. Collectively, the observed differential impact of the Dicer deficiency on microglia highlights the profound changes this tissue macrophage compartment undergoes with time.

RESULTS

Microglia Display a Distinct MicroRNA Profile Compared to Other Tissue Macrophages

To investigate a potential link of miRNAs to microglia identity, we profiled the miRNA repertoire (miRNome) of adult microglia and compared it to that of peripheral tissue macrophages, including intestinal and liver macrophages (Kupffer cells [KCs]) (Figure S1A). Among 160 miRNAs expressed by microglia, 76 were shared with one or both reference populations (Figure 1A, clusters II, III; Figure S1C), while 84 miRNAs were specific or enriched in microglia, as also confirmed for selected miRNAs by quantitative real-time (qRT)-PCR analysis (Figure 1A, cluster I, Figures 1B and S1B). This included miR-99a-5p, miR-125b-5p, and miR-342-3p, shown to be induced in cultured microglia by TGFβ (Butovsky et al., 2014) and considered part of the tissue imprint establishing microglia identity (Gosselin et al., 2014). The microglia miRNome further comprised miRNAs reported to control microglial activation after inflammation or injury, such as let-7c-5p, let-7i-5p, and miR-181c-5p (Banerjee et al., 2013; Zhang et al., 2012). Microglia, moreover, shared expression of other inflammation-associated miRNAs, such as miR-146a-5p (Saba et al., 2012; Taganov et al., 2006) with colonic macrophages (cluster III, Figure 1A) and let-7a-5p and let-7d-5p (Iliopoulos et al., 2009) with both KCs and intestinal macrophages (Figure S1C). Overall, this establishes that adult microglia display a specific miRNA signature (Figure 1C), including miRNAs associated with tissue imprint and control of cell activation, that is distinct from that of other tissue macrophages.

To test whether post-transcriptional control by miRNAs contributes to adult microglia maintenance and function, we generated mice lacking Dicer in these cells. Specifically, we crossed *Dicer^{fl}* mice (Harfe et al., 2005) with *Cx3cr1^{CreER}* animals, in which Cre recombinase activity can be induced in microglia and selected other tissue macrophages by tamoxifen (TAM) administration (Goldmann et al., 2016, 2013; Wolf et al., 2017; Yona et al., 2013). *Dicer*-deficient mice die in utero, whereas het-

erozygote mutants are viable without overt phenotype (Bernstein et al., 2003). To increase mutagenesis efficiency, this study was performed on a *Cx3cr1^{CreER}:Dicer$^{fl/-}$* background.

Cx3cr1^{CreER}:Dicer$^{fl/-}$ and control mice were treated with five consecutive TAM injections at the age of 4 weeks (Figure 1D). PCR analysis of genomic DNA isolated from sorted microglia of *Cx3cr1^{CreER}:Dicer$^{fl/-}$* and control mice 6 weeks after TAM treatment confirmed efficient rearrangement of the "floxed" allele (Figure 1E). qRT-PCR analysis at the same time point revealed the essential absence of miRNAs from mutant microglia (Figure 1F). Maturation of miR-451a-5p, which is Dicer independent but relies on the endonuclease Argonaute 2 (*Ago2*) (Cheloufi et al., 2010), was unaffected, indicating that the observed miRNA reduction is specific to the *Dicer* loss.

Dicer Is Largely Dispensable for Steady-State Maintenance of Adult Microglia

Cx3cr1^{CreER}:Dicer$^{fl/-}$ mice harboring miRNA-depleted microglia did not develop any overt phenotype, up to 3 months after TAM treatment. To examine the effect of the miRNA deficiency on microglia homeostasis, including cell numbers and morphology, we performed a histological brain analysis of the animals. *Cx3cr1^{CreER}:Dicer$^{fl/-}$* mice displayed, as compared to littermate controls, a reduction in microglia numbers in cortex and hippocampus (Figures 2A and 2B). Three-dimensional morphometric measurements of *Cx3cr1^{CreER}:Dicer$^{fl/-}$* microglia revealed no significant changes in length of processes or numbers of segments and branch points, though filament dendrite volumes were slightly increased (Figures 2C and 2D). As ramified morphology can be taken as proxy for a resting state of microglia (Harry, 2013; Lawson et al., 1992), this indicated that *Dicer*-deficient microglia are not primed or activated. To test motility and tissue surveillance of the mutant microglia in vivo, we introduced a conditional reporter allele into the animals and monitored fine microglial processes in the intact brain of living mice (Fuhrmann et al., 2010). Analysis of microglial process dynamics revealed only a very subtle, though consistent, reduction of the process turnover rate in *Cx3cr1^{CreER}:Dicer$^{fl/-}$* mice (Figures S1D and S1E). Taken together, miRNA absence from adult microglia did not result in overt spontaneous in situ activation of the cells, although it affected microglia numbers.

The specific miRNome of adult microglia suggested that miRNAs modulate the steady-state microglia transcriptome. Accordingly, comparative RNA-seq analysis of microglia isolated from TAM-treated *Cx3cr1^{CreER}:Dicer$^{fl/-}$* mice and littermate controls revealed 183 upregulated and 128 downregulated genes (with >1.5-fold change [0.6 log2 ratio]) and p < 0.05; Figure 3A). Functional categorization by ingenuity pathway analysis (IPA) for top canonical pathways (p < 0.05, Abs [Z score] < 0.05) and the DAVID bioinformatics database (Dennis et al., 2003) for Gene Ontology annotation of enriched biological processes (p < 0.05) showed altered genes to be associated with cell adhesion and motility, among others (Figures S2A and S2B). The "cell adhesion" category included expression of genes, such as *Cd47*, *Cd34*, *Nid2*, and *Scarb1* and the "integrin signaling"

(F) Diagram summarizing qRT-PCR analysis for expression of selected miRNAs in microglia sorted from brains of *Cx3cr1^{CreER}:Dicer$^{fl/-}$* and *Cx3cr1^{CreER}:Dicer$^{+/-}$* mice, 6 weeks after TAM treatment. Data are from one experiment including n = 3 of both controls (*Cx3cr1^{CreER}:Dicer$^{+/-}$*) and *Cx3cr1^{CreER}:Dicer$^{fl/-}$* mice, statistically analyzed with Student's t test for each miRNA (*p < 0.05).
See also Figures S1A–S1C.
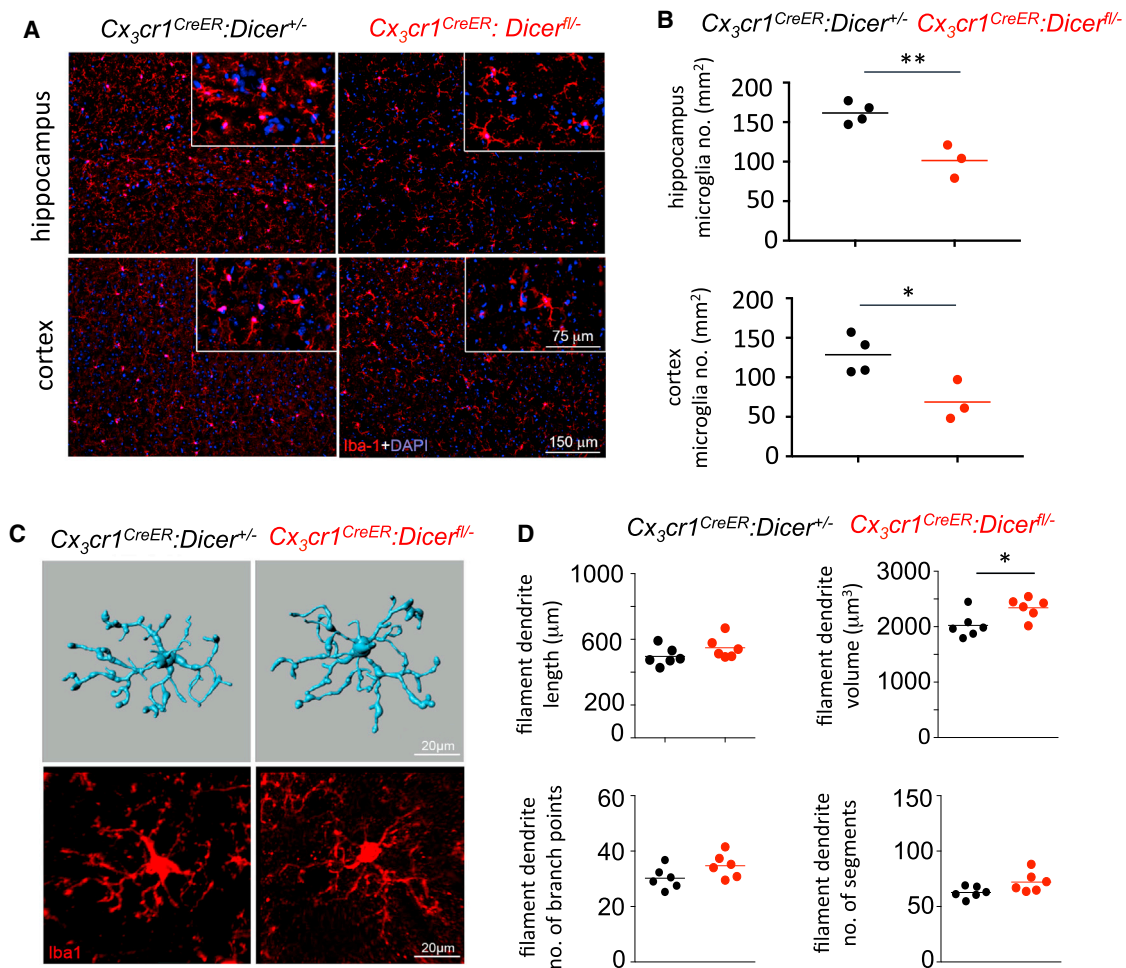
Figure 2. Dicer-Deficient Adult Microglia in Steady State Are Affected in Numbers, but Not Morphology

(A) Histological analysis of cortex and hippocampus of $Cx3cr1^{CreER}:Dicer^{fl/-}$ mice and controls: Iba1 (red), DAPI (blue).

(B) Diagram summarizing microglia densities. Data are from one experiment including $Cx3cr1^{CreER}:Dicer^{+/-}$ (n = 4) and $Cx3cr1^{CreER}:Dicer^{fl/-}$ (n = 3) mice, statistically analyzed with Student's t test (*p < 0.05, **p < 0.01).

(C) Representative three-dimensional reconstruction of cortical microglia morphology of $Cx3cr1^{CreER}:Dicer^{fl/-}$ mice and controls.

(D) Imaris-based automatic quantification of cell morphology. Each symbol represents an average of at least three cells measured in a specific tissue sample. Data represent two independent experiments including $Cx3cr1^{CreER}:Dicer^{+/-}$ (n = 6) and $Cx3cr1^{CreER}:Dicer^{fl/-}$ (n = 6) mice, statistically analyzed with Student's t test (*p < 0.05).

See also Figures S1D and S1E.

category comprised *Itga6*, *ItgaV*, and *Itgb3* (encoding CD61) (Figure 3B). Increased expression of CD34 and CD61 was confirmed by flow cytometry (Figure 3C). In line with the notion that miRNAs fine-tune transcriptomes (O'Connell et al., 2012), overall changes were subtle (only 143 genes ≥ 2-fold change, p < 0.05). Collectively, these data indicate that miRNA absence from adult microglia does not result in their activation.

Dicer-Deficient Microglia Are Hyper-responsive to Systemic LPS Challenge

To explore whether the absence of miRNAs affects microglia responses to inflammatory stimuli, we challenged $Cx3cr1^{CreER}:Dicer^{fl/-}$ mice and control littermates with the bacterial endotoxin lipopolysaccharide (LPS). Specifically, animals were treated with a single intra-peritoneal (i.p.) LPS injection, and brain microglia were isolated 6 hr later in order to perform RNA-seq analysis.

Both control and miRNA-deficient microglia responded robustly (Figures 4A and S3A); 351 genes were found similarly induced in both control and mutant microglia (cluster I, II), including *Myd88*, *Tlr2*, *Cd14*, *Trem1*, and *Tnf*. 172 genes showed less induction in mutant cells (cluster III). Finally, miRNA-deficient microglia displayed prominent hyper-induction of 195 genes (cluster IV), which comprised IL1β-associated genes (*Il1b*, *Il18rap*), the ECM-related pro-inflammatory gene fibronectin 1 gene (*Fn1*), chemokines (*Ccl17*, *Ccl21*), as well as co-stimulatory molecules (*Cd40*, *Cd74*) (Figures 4A and 4B). Overexpression of the pro-inflammatory cytokines *Il1b* and *Il6* as well as *Il18rap* and *Fn1* by mutant microglia after systemic LPS challenge was validated by qRT-PCR analysis (Figures 4C and S3B). Increased surface expression of CD40 and CD11b (*Itgam*) by mutant cells was confirmed by flow cytometric analysis and was evident even before LPS exposure (Figure 4D). Confirming
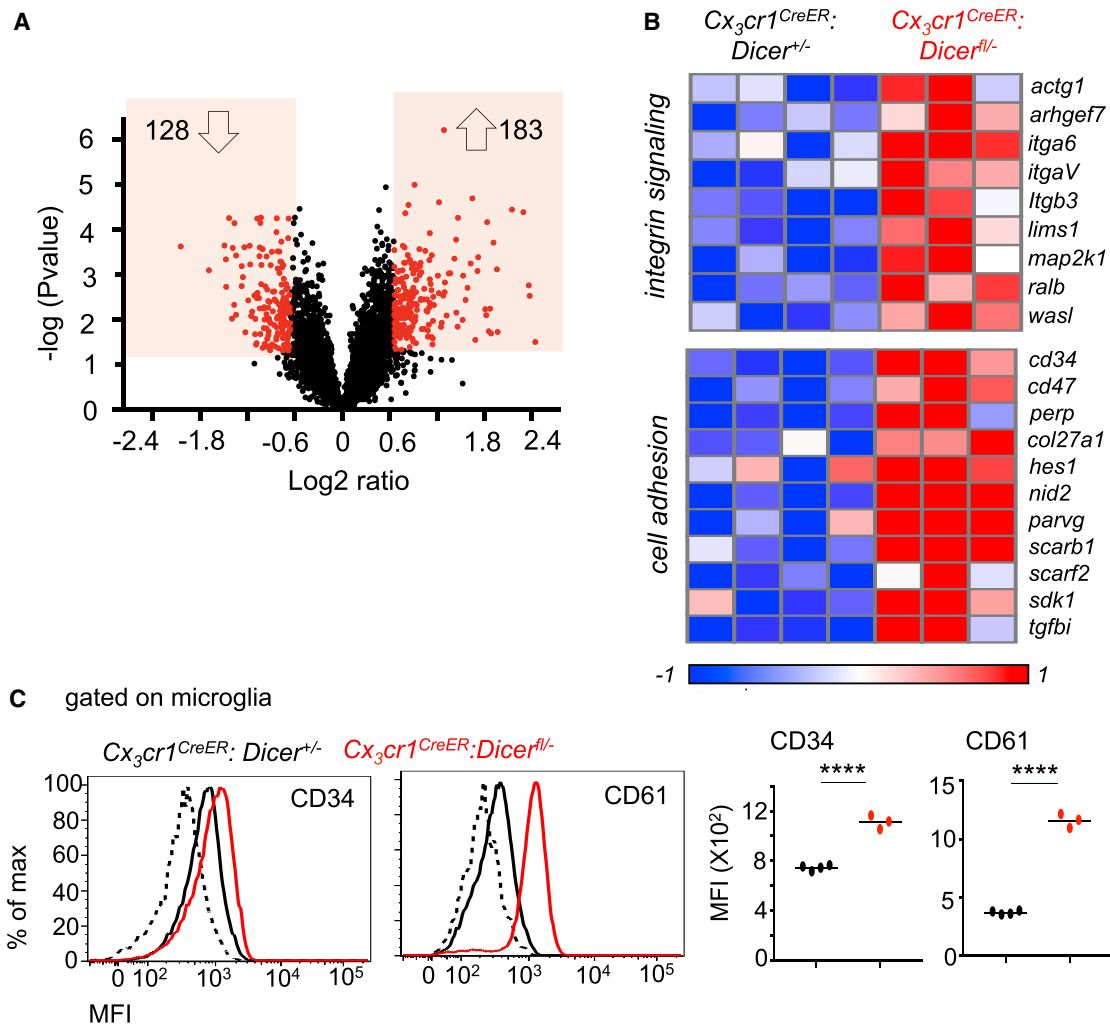
Figure 3. Microglia of TAM-Treated Adult *Cx3cr1^CreER^:Dicer^fl/−^* Mice Do Not Show Overt Activation

(A) Volcano plot of statistical significance (−log10 p value) against log2 ratio between *Cx3cr1^CreER^:Dicer^fl/−^* and *Cx3cr1^CreER^:Dicer^+/−^* control mice, based on the RNA-seq data (log2 ratios and statistics were performed by Deseq program). Significantly changed genes (>1.5-fold change [0.6 log2 ratio, p value < 0.05]) are represented by red symbols. *Cx3cr1^CreER^:Dicer^fl/−^* (n = 3), *Cx3cr1^CreER^:Dicer^+/−^* (n = 4). These results are representative of two independent experiments, total n = 6 (*Cx3cr1^CreER^:Dicer^fl/−^*), n = 7 (*Cx3cr1^CreER^:Dicer^+/−^*), see PBS controls in Figure 4A (PBS controls).

(B) Heatmap analysis showing log2 transformed standardized and normalized read numbers of upregulated genes associated with selected functional cate-gorization presented in Figures S2A and S2B, based on ingenuity pathway and Go annotation analysis for biological process of the samples in (A).

(C) Flow cytometry analysis of microglial CD61 and CD34 surface expression levels (mean fluorescence intensity [MFI]), isolated from TAM-treated *Cx3cr1^CreER^:Dicer^fl/−^* mice (red; n = 3) and controls (black; n = 4), statistically analyzed with Student's t test (*p < 0.05).

See also Figure S2.

the general role of miRNAs in curbing microglia activation, micro-glia were also found hyper-responsive to a systemic challenge by the dsRNA mimic polyinosinic:polycytidylic acid (poly(I:C)) (Figure S3B).

To identify miRNAs, whose absence might be responsible for the transcriptome dysregulation in *Dicer*-deficient microglia after the LPS challenge, we aligned the upregulated genes with a list of conserved miRNA targets (Figures S3C and S3D). Ten miRNAs passed the significance threshold of the two tests we used (hypergeometric test, GSEA software analysis). Interest-ingly, six of these miRNAs were expressed in steady-state microglia (Figures 1A, 4E, S1B, and S1C). miR-126a-3p, on the other hand, a miRNA absent from the steady-state microglia,

was induced after LPS challenge (Figure 4F). Taken together, these data establish that Dicer-deficient microglia hyper-respond to a peripheral LPS challenge, corroborating the critical role of miRNAs in controlling inflammation.

Hyper-active Dicer-Deficient Microglia Acutely Impair Hippocampal Neuronal Functions

Systemic endotoxin challenge was shown to transiently impair the response of hippocampal neurons to repeated synapse stim-ulation (Maggio et al., 2013; Strehl et al., 2014; Vereker et al., 2000). Specific microglia contributions to this phenomenon of impaired hippocampal long-term potentiation (LTP) are not yet established.
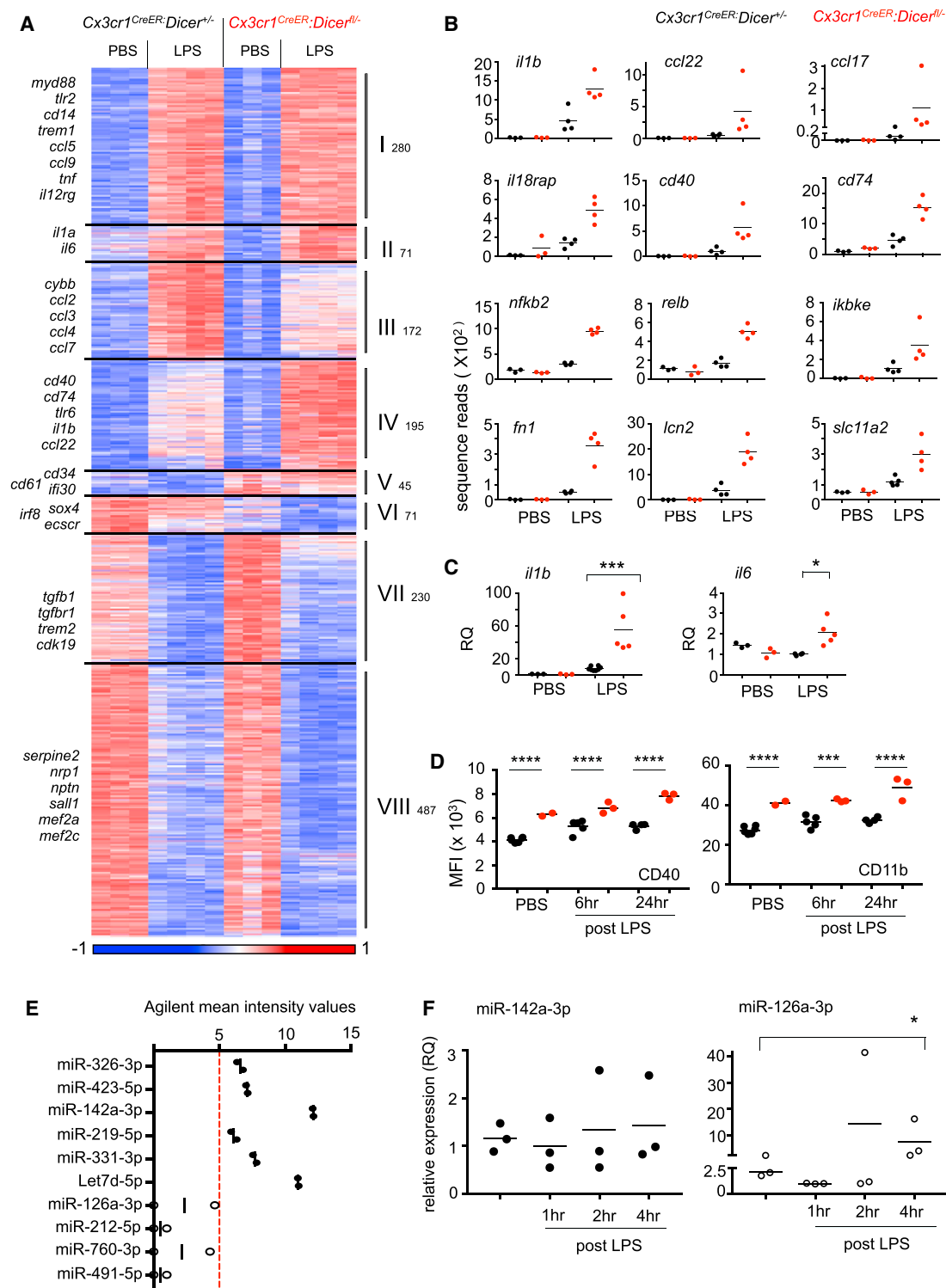
Figure 4. Dicer-Deficient Microglia Are Hyper-responsive to Systemic LPS Challenge

(A) Heatmap analysis of mRNA profiles of microglia isolated from PBS or LPS-treated *Cx3cr1^CreER^:Dicer^fl/−^* and control mice 6 hr after treatment. Genes displayed represent a statistically significant ≥2-fold change between any two of the groups (1,551 genes) (log2 ratios and statistics were performed by Deseq program). Normalized read numbers were log-transformed and standardized. Genes were clustered by a Pearson correlation test and number of partition clusters was set to eight. Data are from one experiment including *Cx3cr1^CreER^:Dicer^+/−^* PBS mice (n = 3), *Cx3cr1^CreER^:Dicer^+/−^* LPS mice (n = 4), *Cx3cr1^CreER^:Dicer^fl/−^* PBS mice (n = 3), and *Cx3cr1^CreER^:Dicer^fl/−^* LPS mice (n = 4).

(B) Examples of gene expression as identified in cluster IV (Figure 4A). Shown are the mean sequence reads.

(legend continued on next page)

Dicer-deficient hippocampal microglia displayed a hyper-activation response that largely overlapped with the response of whole brain mutant microglia, including increased expression of *Il1b* and co-stimulatory molecules (Figures 5A, 5B, 4A, S4A, and S4B, Table S1). As previously shown (Vereker et al., 2000), LPS challenge led to induction of pro-IL-1β protein in the hippocampus (Figure 5C). Moreover, hyper-activation of *Dicer*-deficient microglia was reflected in increased pro-IL-1β protein expression 6 hr after the LPS treatment (Figure 5D). To test a potential impact of the mutant hyperactive microglia on neuronal fitness, we performed extracellular recordings on acute slices prepared from dorsal hippocampi of the animals (Strehl et al., 2014) and examined LTP 12 and 24 hr after LPS stimulus (Figure 5E). *Cx3cr1*^{CreER}:*Dicer*$^{fl/-}$ mice presented unaltered baseline synaptic transmission and excitatory synaptic strength, as compared to controls (Figure S4C). LTP of all mice was reduced by 12 hr after LPS challenge, but the neuronal response of TAM-treated mutant *Cx3cr1*^{CreER}:*Dicer*$^{fl/-}$ animals was significantly more affected (Figures 5F and S4D). In line with the reported transient nature of the effect, control mice displayed partial LTP recovery by 24 hr; *Cx3cr1*^{CreER}:*Dicer*$^{fl/-}$ animals, however, showed persistent LTP reduction (Figures 5F and S4D). Overall, these results suggest that hyper-activation of *Dicer*-deficient microglia after peripheral LPS challenge results in prolonged hippocampal LTP impairment and acutely affects neuronal circuits.

Prenatal Dicer Mutagenesis Induces DNA Damage in Newborn Microglia and Renders Microglia Radio-sensitive

Unlike in the adult, microglia in the developing CNS are highly proliferative and migratory and display profound phagocytic activity (Harry, 2013; Orłowski et al., 2003). This is in line with the critical contributions of embryonic microglia to the establishment and maturation of neuronal circuits (Paolicelli et al., 2011; Schafer et al., 2012; Squarzoni et al., 2014). Embryonic (E14) and newborn (P0) microglia display transcriptomes that are profoundly distinct from adult microglia, with one fifth of the expression signature specific for the respective stage (Figures 6A and 6B; see also Kierdorf et al., 2013; Mass et al., 2016; Matcovitch-Natan et al., 2016). Establishment of "relative quiescence" in adult microglia was proposed to be related to their expression of the zinc finger transcriptional repressor Sall1 (Buttgereit et al., 2016). In line with their reported activity, E14 and P0 microglia

expressed cell cycle-associated genes, including *Cks1b*, *Cdc25a*, and *Cdk1* (Figures 6A and S5A). Moreover, E14 and P0 microglia displayed signs of an oxidative stress response (*cdc34*, *ftl1*, *hmox1*, *prdx1*) (cluster II), suggesting ROS production, as also supported by high NADPH oxidase (Nox2) expression (*cybb*) of E14 microglia (cluster I, Figure 6A).

Given the functional differences between neonatal and adult microglia, we decided to probe the effect of the Dicer deficiency on pre- and neonatal microglia by generating *Cx3cr1*^{Cre}:*Dicer*$^{fl/fl}$ mice (Harfe et al., 2005; Yona et al., 2013). In these animals, Cre recombinase is expressed at day E7.5 in primitive CX$_3$CR1$^+$ yolk sac macrophages that give rise to microglia (Figure 6C; Bertrand et al., 2005; Ginhoux et al., 2010). miRNA absence in microglia of adult 6-week-old *Cx3cr1*^{Cre}:*Dicer*$^{fl/fl}$ mice was validated by qRT-PCR analysis (Figure 6D). Gene expression profiling at P0 revealed that *Dicer*-deficient cells displayed 159 up- and 256 downregulated genes (out of a total of 8,545 genes), as compared to controls (Figure 6E). *Dicer*-deficient P0 microglia showed prominent induction of the "DNA damage response" pathway (Figure S5B), as manifested by upregulation of *Cdkn1a*, *Cdkn2d*, *Ddit4*, and *Dst* (Figures 6F and 6G). Moreover, concomitant reduction of the "cyclins and cell cycle" pathway, including expression of *Ccnb1*, *Cdk4*, and *Mcm2* (Figures 6F, cluster II, and S5A), suggested that mutant microglia respond to accumulated DNA damage by cell cycle arrest (Zhou and Elledge, 2000). Indeed, 5-ethynyl-2′-deoxyuridine (EDU) labeling and Ki67 staining revealed that the frequency of proliferating newborn microglia was significantly reduced in *Cx3cr1*^{Cre}:*Dicer*$^{fl/fl}$ mice, as compared to littermate controls (Figures 6H, S5C, and S5D).

To directly examine DNA integrity of *Dicer*-deficient microglia, we performed a gel electrophoresis-based "comet assay" that allows visualization of single- and double-strand DNA breaks on a single-cell level (Olive and Banáth, 2006). As shown in Figure 7A, microglia sorted from brains of newborn *Cx3cr1*^{Cre}:*Dicer*$^{fl/fl}$ mice, but not littermate controls, displayed significant DNA damage. This suggested that newborn *Dicer*-deficient microglia are unable to repair endogenous DNA damage potentially resulting from their prominent replication or ROS production (McKinnon, 2013; Zhou and Elledge, 2000), a phenotype that might relate to miRNA-independent Dicer involvement in DNA repair (Francia et al., 2012; Wei et al., 2012).

Microglia are characterized by profound resistance to ionizing radiation (Mildner et al., 2007). To test whether lack of Dicer and

(C) Graphical summary of qRT-PCR analysis showing relative quantities of mRNA for *il6* and *il1b* in microglia sorted 6 hr after an i.p. injection of either PBS or LPS of TAM-treated *Cx3cr1*^{CreER}:*Dicer*$^{fl/-}$ and control mice. Data are statistically analyzed with one-way ANOVA for multiple comparisons (*p < 0.05, ***p < 0.001). *Cx3cr1*^{CreER}:*Dicer*$^{+/-}$ PBS (n = 3), *Cx3cr1*^{CreER}:*Dicer*$^{fl/-}$ PBS (n = 3), *Cx3cr1*^{CreER}:*Dicer*$^{+/-}$ LPS (n = 4), *Cx3cr1*^{CreER}:*Dicer*$^{fl/-}$ LPS (n = 5). Data are representative of two independent experiments.

(D) Graphical summary of surface expression of CD40 and CD11b on microglia isolated from *Cx3cr1*^{CreER}:*Dicer*$^{fl/-}$ and control mice after i.p. injection of either PBS or LPS. Data are expressed as mean fluorescence intensity and statistically analyzed with one-way ANOVA for multiple comparisons (***p < 0.001, ****p < 0.0001). Data are from one experiment including *Cx3cr1*^{CreER}:*Dicer*$^{+/-}$ PBS (n = 6), *Cx3cr1*^{CreER}:*Dicer*$^{fl/-}$ PBS (n = 2), *Cx3cr1*^{CreER}:*Dicer*$^{+/-}$ 6 hr LPS (n = 5), *Cx3cr1*^{CreER}:*Dicer*$^{fl/-}$ 6 hr LPS (n = 3), *Cx3cr1*^{CreER}:*Dicer*$^{+/-}$ 24 hr LPS (n = 4), *Cx3cr1*^{CreER}:*Dicer*$^{fl/-}$ 24 hr LPS (n = 3).

(E) Graphical summary of expression level of miRNAs predicted to target genes upregulated in *Cx3cr1*^{CreER}:*Dicer*$^{fl/-}$ microglia in response to LPS (see table in Figure S3C, summarizing results obtained from two statistical tests used for miRNA prediction). Shown are mean intensity values for steady-state expression of each miRNA in WT microglia, as measured in Agilent microarray (Figures 1A, S1B, and S1C), either expressed (filled bars) or absent (below minimal array detection intensity level of 5) in steady state (open bars).

(F) Expression level measured by qRT-PCR of miR142a-3p and miR126a-3p in WT microglia non-treated, 1 hr, 2 hr, and 4 hr after LPS i.p injection; miRNA expressed in steady state (filled); miRNA absent in steady state (open); data are statistically analyzed with Student's t test (*p < 0.05). Data are from one experiment, n = 3 per time point.

See also Figure S3.
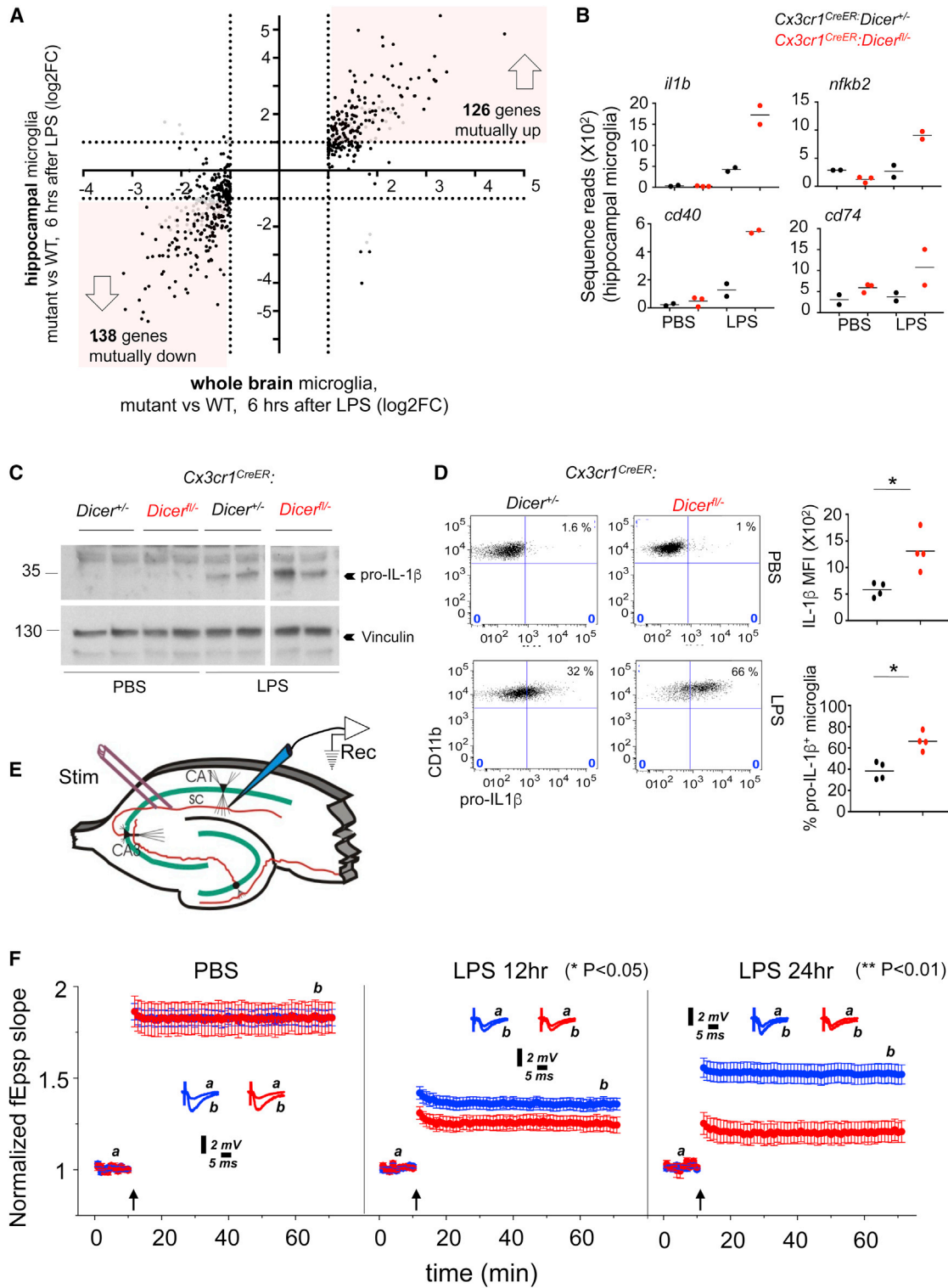
Figure 5. Hyper-active Dicer-Deficient Microglia Impair Hippocampal Neuronal Functions after LPS Exposure

(A) Comparison of gene expression log2 ratios between *Cx3cr1^CreER^:Dicer^fl/−^* and control hippocampal and whole-brain microglia, 6 hr after 1 mg/kg LPS i.p. injection. Similarity of mutant microglia is indicated by Pearson correlation test (r = 0.856); whole-brain *Cx3cr1^CreER^:Dicer^+/−^* 6 hr LPS (n = 4), whole-brain *Cx3cr1^CreER^:Dicer^fl/−^* 6 hr LPS (n = 4), hippocampal *Cx3cr1^CreER^:Dicer^+/−^* 6 hr LPS (n = 2), hippocampal *Cx3cr1^CreER^:Dicer^fl/−^* 24 hr LPS (n = 2). See Table S1 for detailed gene lists. Whole brain significantly changed gene expression log2 ratios (log2 ratio of >1 or <−1, p < 0.05) 6 hr after 1 mg/kg LPS i.p. injection served as

(legend continued on next page)

the associated impaired DNA repair renders these cells radio-sensitive, we irradiated *Cx3cr1^Cre^:Dicer^fl/fl^* and control mice (950 rad) and analyzed the frequency of apoptotic microglia cells. Irradiated *Dicer*-deficient microglia comprised significantly more late apoptotic events than controls, indicating increased radio-sensitivity (Figures 7B and S6A). Next, we lethally irradiated *Cx3cr1^Cre^:Dicer^fl/fl^* mice and controls at P0 or at 4 weeks of age and reconstituted them with bone marrow (BM) isolated from *Cx3cr1^gfp^* reporter animals (Jung et al., 2000). In line with microglial radio-resistance, brain macrophage compartments of control chimeras showed only minor engraftment, even when irradiated newborns were used as recipients (Figures 7C and 7D). In contrast, Dicer-deficient microglia were quantitatively replaced by *Cx3cr1^gfp^* BM-derived cells in the chimeric mice (Figures 7C and 7D). Importantly, radio sensitivity was a general feature of Dicer-deficient microglia. Thus, adult TAM-treated *Cx3cr1^CreER^:Dicer^fl/−^* animals, when irradiated and engrafted with WT BM, also showed significant replacement of their microglia by graft-derived macrophages (Figure S6B). However, WT BM engraftment efficiency was dependent on the time interval between TAM treatment and BM engraftment, with larger time intervals showing reduced efficiency (Figure S6B). This indicates a progressive loss of mutant microglia in these animals, as also highlighted by the declining frequency of *Dicer*-null allele in sorted *Cx3cr1^CreER^:Dicer^fl/−^* microglia over time (Figure S6C). Mutant microglia thus have a disadvantage over residual WT cells, which harbor profound expansion potential (Bruttger et al., 2015). Collectively, these data establish a critical role of Dicer in microglial repair of endogenously or exogenously induced DNA damage.

Finally, we found that adult *Cx3cr1^Cre^:Dicer^fl/fl^* animals but not TAM-treated *Cx3cr1^CreER^:Dicer^fl/−^* mice displayed sporadic pathologies, including impaired dental growth (data not shown), likely due to the impairment of other tissue macrophage populations in these animals. Indeed, the dicer deficiency resulted in depletion of selected additional cells, such as Langerhans' cells (LCs), as previously reported (Turner et al., 2011), and dendritic epidermal T cells (DETCs) (Figures S6D and S6E). Microglia of adult *Cx3cr1^Cre^:Dicer^fl/fl^* mice exhibited an activated morphology characterized by an amoeboid shape and increased cell body

size, as compared to littermate controls (Figures S7A–S7C). Microglia densities measured in the cerebellum, cortex, and spinal cord were, however, largely unaltered (Figure S7D). By the age of 6 to 8 weeks, all *Cx3cr1^Cre^:Dicer^fl/fl^* animals developed a motoric hind leg deficiency (Figures S7E–S7G). Prenatal absence of Dicer, Dicer-dependent regulatory miRNAs, or other ncRNAs from microglia could thus have a long-term effect associated with CNS dysfunction, although the mechanism underlying this phenomenon and its direct link to the microglia impairment remain to be elucidated.

DISCUSSION

Recent studies highlighted the impact of the local tissue environment on macrophage identities (Gosselin et al., 2014; Lavin et al., 2014); however, mechanisms that establish and maintain specific expression signatures remain incompletely understood (Amit et al., 2016). Here, we investigated the role of Dicer and Dicer-dependent ncRNAs, such as miRNAs, in microglia biology. Specifically, we used two complementary experimental systems to ablate the *Dicer* gene either during microglia development or in adulthood. We show that the same genetic perturbation has a differential impact on these cells in the adult and developing brain, since microglia are in different functional states within these time windows.

Despite the characteristic miRNome of adult microglia and the notion that lack of miRNAs increases protein expression noise (Schmiedel et al., 2015), we found Dicer and its products largely dispensable for the maintenance of adult microglial function under physiological conditions, including their characteristic morphology and extension dynamics. Specifically, Dicer-deficient adult microglia did not show signs of spontaneous activation; however, they did display a reduced tissue density and were in steady state progressively, albeit slowly, out-competed by rare Dicer-proficient cells.

miRNAs have an established role in controlling cellular activation (O'Connell et al., 2012). Accordingly, the absence of miRNAs from microglia resulted in profound hyper-activation of these cells after peripheral challenges, including LPS and poly(I:C). The microglial steady-state miRNome comprises miRNAs

---

the standard, to which the hippocampal microglia gene expression log2 ratios under the same condition were aligned. Grey dots represent hippocampal microglia log2 ratios that were either >1 or <−1 but not statistically significant (p > 0.05).

(B) Examples of gene expression for genes mutually upregulated 6 hr after LPS in both whole-brain and hippocampus microglia from *Cx3cr1^CreER^:Dicer^fl/−^* mice compared to *Cx3cr1^CreER^:Dicer^+/−^* mice (shown in A). Shown are the mean sequence reads of hippocampal microglia (see full RNA-seq analysis of hippocampal *Cx3cr1^CreER^:Dicer^fl/−^* compared with controls, either at steady state or 6 hr after i.p. injection of LPS 1 mg/kg in Figures S4A and S4B).

(C) Western blot analysis of hippocampal extracts of unchallenged and LPS-challenged *Cx3cr1^CreER^:Dicer^fl/−^* mice and littermate controls (*Cx3cr1^CreER^:Dicer^+/−^*) for expression of pro-IL1β protein, non-treated and 6 hr after LPS i.p. injection. n = 2 per group. Data are a representative of two independent experiments, total n = 4.

(D) Flow cytometric analysis of microglia isolated from unchallenged and LPS-challenged *Cx3cr1^CreER^:Dicer^fl/−^* mice and littermate controls (*Cx3cr1^CreER^:Dicer^+/−^*) for expression of pro-IL1β protein, 6 hr after LPS i.p. injection. Data are statistically analyzed with Student's t test (*p < 0.05). *Cx3cr1^CreER^:Dicer^fl/−^* (n = 4), *Cx3cr1^CreER^:Dicer^+/−^* (n = 4). Data are a representative of two independent experiments, total n = 9 (*Cx3cr1^CreER^:Dicer^fl/−^*), n = 7 (*Cx3cr1^CreER^:Dicer^+/−^*).

(E) Graphical description of LTP measurement protocol. Stimulation of Schaffer's collaterals was evoked using a pulse stimulator and delivered through a bipolar nichrome electrode.

(F) LTP analysis on Schaffer collateral cornu ammonis 1 (CA1) region synapses probed in acute hippocampal slices isolated from either 12 hr post PBS-, 12 hr post LPS-, or 24 hr post LPS-treated *Cx3cr1^CreER^:Dicer^fl/−^* mice and controls. Averaged EPSP are plotted versus time. Data are expressed as mean ± SEM and statistically analyzed with two-way ANOVA on time point 60 considering the type of treatment, genotype, and the interaction between the two factors (*p < 0.05, **p < 0.01 represent the significance of interaction). Representative traces at indicated times (a, b) are shown on top of each section. Upward arrows indicate the time of high-frequency stimulation (HFS). *Cx3cr1^CreER^:Dicer^+/−^* PBS, 12 hr, 24 hr LPS (n = 4 each); *Cx3cr1^CreER^:Dicer^fl/−^* PBS (n = 3), 12 hr (n = 4), 24 hr LPS (n = 4). Of note, an independent duplicate experiment, including an additional WT group, is shown in Figure S4D.

See also Figure S4.
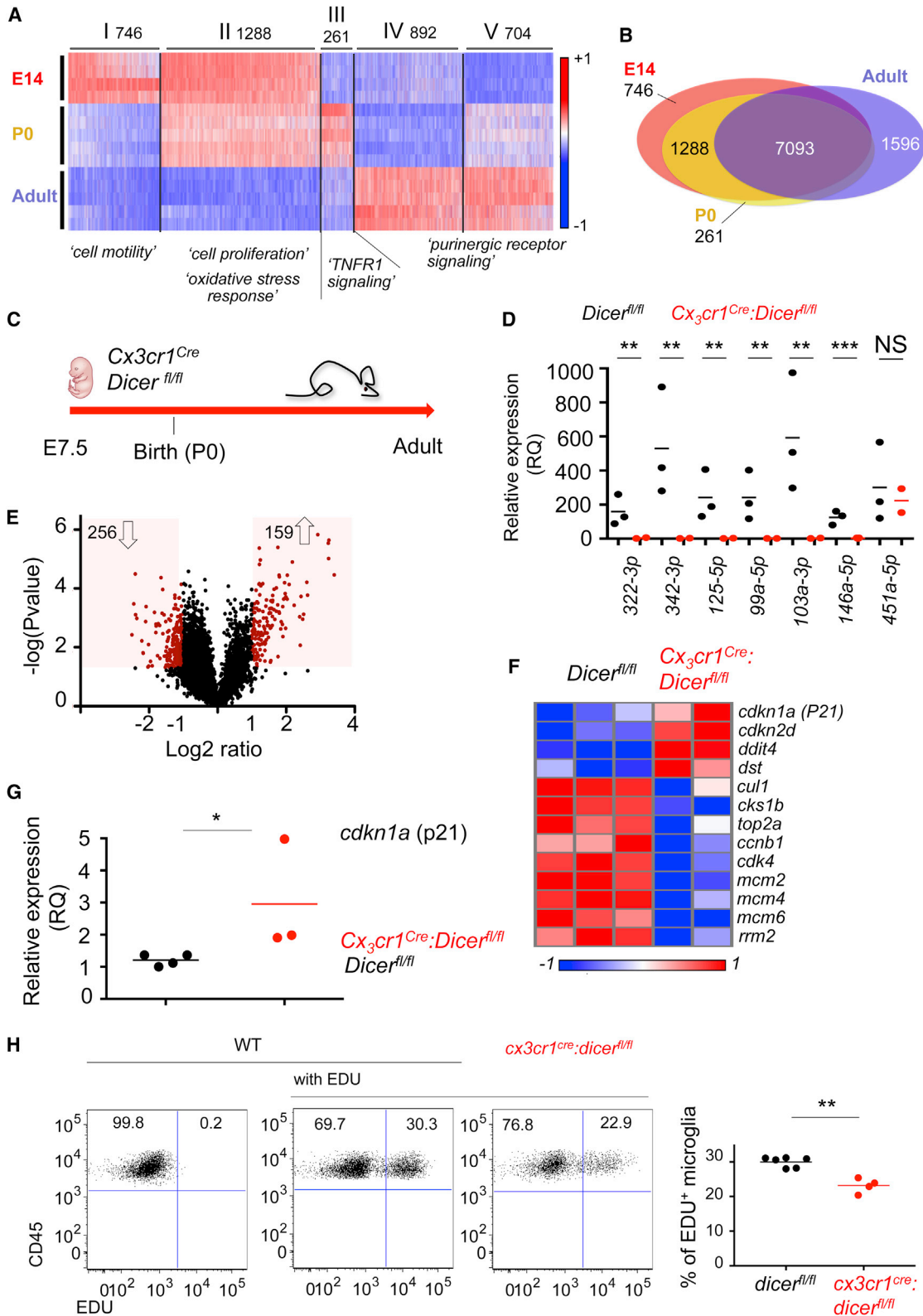
Figure 6. After Prenatal *Dicer* Mutagenesis, Newborn Microglia Display a DNA Damage Response and Cell Cycle Arrest

(A) Heatmap analysis of mRNA profiles of microglia sorted from embryonic day 14 (E14), newborns (P0), and adult (6-week-old) mice. Genes were filtered for ≥2-fold statistically significant change between any pair of samples (3,891 genes) (log2 ratios and statistics were performed by Deseq program). Normalized

(legend continued on next page)

predicted to target 3′ UTRs of pro-inflammatory genes, such as *Il1b*, including miRNA-331-3p and miRNA-125b-5p. Moreover, microglia challenge induces expression of additional miRNAs that shape pro-inflammatory responses, including miR-155, miR-223, miR-218, and miR-194 (Butovsky et al., 2012), as well as miR-126a-3p, shown in this study. The latter targets the inflammatory response genes *Nfkb2* and *Slc11a2* (Cellier et al., 2007; Mancino et al., 2013), which we found increased in the *Dicer* mutant microglia after LPS treatment. The observed challenge-induced hyperactivation of Dicer-deficient microglia probably results from the combined absence of steady-state and induced anti-inflammatory miRNAs, as also indicated by our bio-informatic analysis. Moreover, in addition to miRNA maturation, Dicer has been implicated in the processing of other ncRNAs involved in regulating the immune response. The latter include toxic Alu/B1/B2 ncRNAs (Kaneko et al., 2011), which accumulate in Dicer absence and activate the NLRP3 inflammasome (Gelfand et al., 2015). Such miRNA-independent mechanisms might contribute to the fact that microglia of *Cx3cr1^Cre^:Dicer^fl/fl^* and TAM-treated *Cx3cr1^CreER^:Dicer^fl/−^* mice show hyper-activation, either spontaneously or after challenge.

Peripheral endotoxin challenge results in a neuro-inflammatory response and transient impairment of hippocampal LTP (Vereker et al., 2000). More specifically, pro-inflammatory cytokines, such as TNF and IL-1β, were shown to affect glutamate receptors activity in the CA1 area of the hippocampus (Riazi et al., 2015); however, the specific effect of microglia activation on the stimulation of CA1 pyramidal neurons and the resulting LTP response in vivo was not examined so far. Here we show that TAM-treated *Cx3cr1^CreER^:Dicer^fl/−^* mice displayed, as compared to littermate controls, a significantly weakened hippocampal neuron response to repeated synapse stimulation, as well as delayed recovery. *Cx3cr1^CreER^:Dicer^fl/−^* mice might thus provide a valuable model to study the interplay of hyper-activated microglia with hippocampal astrocytes and neurons in the context of the LTP response, and define molecular parameters of their cellular crosstalk, including the role of TNF (Habbas et al., 2015). Of note, in *Cx3cr1^CreER^:Dicer^fl/−^* mice, also non-parenchymal CNS macrophages are targeted (Goldmann et al., 2016). Although we established a cell-intrinsic effect of the *Dicer* mutation in isolated microglia, we cannot rule out that mutagen-

esis of these populations contributes as well to the LTP impairment. Future studies should also address the impact of microglia hyper-activation on cognitive and associative memory characteristics and behavioral comorbidities, such as seen in patients exposed to acute infections.

Dicer promotes cell survival and its absence can result in cell death, as shown for neurons, glia, and immune cells (Kim et al., 2009; Koralov et al., 2008; Kuipers et al., 2010; Schaefer et al., 2007; Tao et al., 2011). Accordingly, *Cx3cr1^Cre^:Dicer^fl/fl^* mice also lacked selective cell populations that express CX₃CR1 either during development (LCs) or upon maturation (DTECs). Microglia tissue density and motility were reduced in both hippocampus and cortex of TAM-induced *Cx3cr1^CreER^:Dicer^fl/−^* mice, as compared with WT mice, indicating an effect on microglia network connectivity and survival. Moreover, in TAM-treated *Cx3cr1^CreER^:Dicer^fl/−^* mice, mutant cells were over time slowly outcompeted by *Dicer*-proficient microglia. *Dicer*-dependent cell survival is likely related to a critical role of Dicer in DNA repair and preservation of genome integrity (Swahari et al., 2016), including in response to γ irradiation-induced DNA damage (Francia et al., 2012; Wei et al., 2012). In support of this notion, otherwise radio-resistant microglia were rendered radio sensitive by the Dicer deficiency, both at the perinatal and adult stages, as demonstrated in *Cx3cr1^Cre^*- and *Cx3cr1^CreER^:Dicer^fl^* mice. Dicer deficiency in development, a stage where microglia are highly proliferative and active and thus exposed to endogenous genotoxic stress, resulted in a prominent accumulation of DNA damage. In contrast, the need for Dicer in DNA repair in the more quiescent adult microglia was revealed when the cells were damaged by external manipulation, i.e., γ irradiation. Future studies should investigate the long-term impact of the DNA repair defect on microglial genome integrity and the establishment of microglia senescence.

Adult *Cx3cr1^Cre^:Dicer^fl/fl^* mice develop a significant though non-progressive amyotrophic lateral sclerosis (ALS)-like motoric hind leg deficiency. The exact cause of this phenomenon remains unclear. Notably, when combined with certain "floxed" reporter alleles, adult *Cx3cr1^Cre^* mice display rearrangements in neurons (Z. Haimon, D.V., L.C.-M., S.B.-H., and S.J., unpublished data). Adult neurons do not express CX₃CR1, so this is likely due to a yet undefined narrow and transient window of

read numbers were log-transformed and standardized. Genes were clustered by Pearson correlation test, number of partition clusters was set to five. Prominent canonical pathways assigned by ingenuity pathway analysis are indicated for each cluster. Data are pooled from two independent experiments. E14 (n = 4), P0 (n = 5), 6-week-old (n = 5).

(B) Venn diagram illustrating level of transcriptome overlap between prenatal (E14, red), newborn (P0, yellow), and adult (6 week, blue) microglia.

(C) Scheme illustrating E7.5 onset of constitutive microglial mutagenesis in *Cx3cr1^Cre^:Dicer^fl/fl^* mice.

(D) Summary of qRT-PCR analysis for expression of selected miRNAs in microglia sorted from brains of 6-week-old *Cx3cr1^Cre^:Dicer^fl/fl^* and *Dicer^fl/fl^* mice. Data are statistically analyzed with Student's t test. **p < 0.01, NS p > 0.05. *Cx3cr1^Cre^:Dicer^fl/fl^* (n = 2), *Dicer^fl/fl^* mice (n = 3). Data are representative of two independent experiments, total n = 4 (*Cx3cr1^Cre^:Dicer^fl/fl^*), n = 5 (*Dicer^fl/fl^*).

(E) Volcano plot displaying statistical significance ($-\log_{10}$ p value) against the $\log_2$ ratio between sorted microglia isolated from *Cx3cr1^Cre^:Dicer^fl/fl^* and *Dicer^fl/fl^* mice based on RNA-seq data. Significantly changed genes (≥ 2 fold change, p < 0.05) are represented by the red symbols ($\log_2$ ratios and statistics were performed by Deseq program). Data are from one experiment, including *Cx3cr1^Cre^:dicer^fl/fl^* (n = 2) and *Dicer^fl/fl^* mice (n = 3).

(F) Heatmap graphical display of genes of the DNA damage response checkpoint and cell cycle regulation categories, as defined by ingenuity pathway analysis (see also Figure S5B) in microglia isolated from *Cx3cr1^Cre^:Dicer^fl/fl^* and *Dicer^fl/fl^* mice (E). Shown are the standardized $\log_2$ transformed read numbers of significantly changed genes (≥ 2 fold change, p < 0.05). *Cx3cr1^Cre^:Dicer^fl/fl^* (n = 2), *Dicer^fl/fl^* mice (n = 3).

(G) Graphical summary of qRT-PCR analysis for *Cdkn1a* expression (encoding p21). Data are statistically analyzed with Student's t test (*p < 0.05); data are from one experiment; *Cx3cr1^Cre^:Dicer^fl/fl^* (n = 3) and *Dicer^fl/fl^* mice (n = 4).

(H) EDU flow cytometric analysis of microglia isolated from P0 *Dicer^fl/fl^* and newborn *Cx3cr1^Cre^:Dicer^fl/fl^* mice revealed decreased proliferation rate in mutant microglia. Data are statistically analyzed with Student's t test (**p < 0.01); data are from one experiment; *Dicer^fl/fl^* (n = 6), *Cx3cr1^Cre^:Dicer^fl/fl^* (n = 4).

See also Figures S5 and S7.
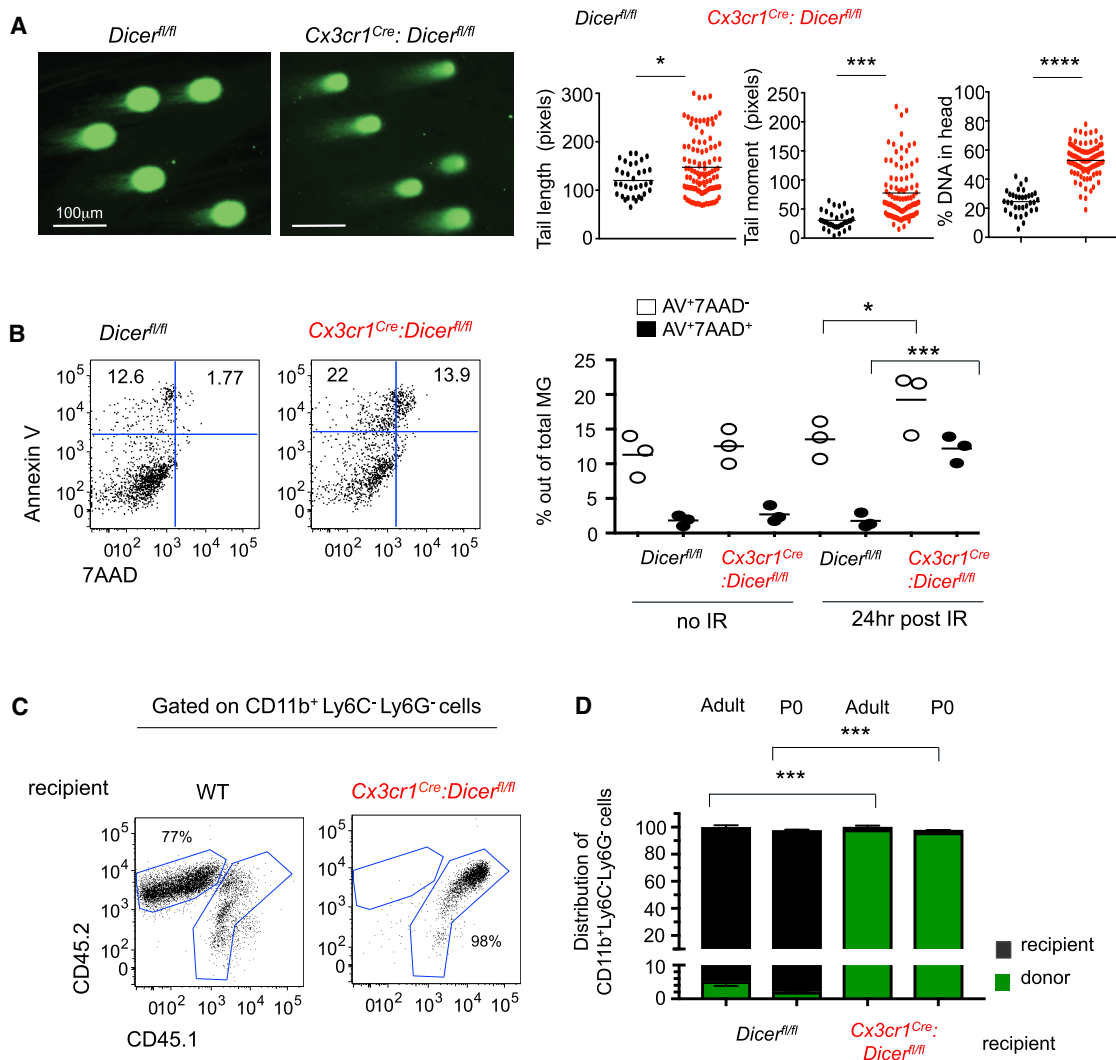
Figure 7. Prenatal Dicer Ablation Causes Accumulation of DNA Damage and Renders Microglia Radio-sensitive

(A) Representative image of comet analysis (left) and a graphical summary (right) of DNA distribution between head and tail of sorted newborn microglia isolated from $Cx3cr1^{Cre}:Dicer^{fl/fl}$ and $Dicer^{fl/fl}$ mice. Data are statistically analyzed with Student's t test (*p < 0.05, ***p < 0.001, ****p < 0.0001). Data are from one experiment, including $Cx3cr1^{Cre}:Dicer^{fl/fl}$ (n = 3) and $Dicer^{fl/fl}$ mice (n = 3).

(B) Representative picture of flow cytometry analysis (left) and a graphical summary (right) of the frequencies for early and late apoptotic microglia of $Cx3cr1^{Cre}:Dicer^{fl/fl}$ and $Dicer^{fl/fl}$ adult mice, which were analyzed untreated or 24 hr after irradiation. Data are statistically analyzed with Student's t test (*p < 0.05, ***p < 0.001); data are from one experiment, n = 3 per group (see also Figure S6A for additional time points).

(C) Representative flow cytometry analysis of brains of [$Cx3cr1^{gfp/+}$ ($CD45.1$) > $Dicer^{fl/fl}$] and [$Cx3cr1^{gfp/+}$ ($CD45.1$) > $Cx3cr1^{Cre}:Dicer^{fl/fl}$] BM chimeras, 6 weeks after transplantation.

(D) Graphical summary of flow cytometry analysis of chimeric mice, including [$Cx3cr1^{gfp/+}$ ($CD45.1$) > $Dicer^{fl/fl}$] and [$Cx3cr1^{gfp/+}$ ($CD45.1$) > $Cx3cr1^{Cre}:Dicer^{fl/fl}$] BM chimeras, performed on either adult or newborn (NB, P0) recipients, 6 weeks after transplantation. Data are from one experiment including [$Cx3cr1^{gfp/+}$ ($CD45.1$) > $Dicer^{fl/fl}$] 6-week-old mice (n = 5), [$Cx3cr1^{gfp/+}$ ($CD45.1$) > $Dicer^{fl/fl}$] NB mice (n = 8), [$Cx3cr1^{gfp/+}$ ($CD45.1$) > $Cx3cr1^{Cre}:Dicer^{fl/fl}$] 6-week-old mice (n = 3), [$Cx3cr1^{gfp/+}$ ($CD45.1$) > $Cx3cr1^{Cre}:Dicer^{fl/fl}$] NB mice (n = 3). Data are expressed as mean ± SEM, statistically analyzed with Student's t test (***p < 0.001).
See also Figure S6.

Cx3cr1 promoter activity during their development. We can therefore not formally exclude that the delayed motor neuron defect in these mice results from Dicer impairment in neurons. Alternatively, the profound cell-intrinsic impairment of the *Dicer*-ablated microglia in the critical time window of CNS development could have a permanent impact on the integrity of neuronal circuits, which might precipitate the delayed pathology.

Collectively, we show the requirement of Dicer and miRNAs for microglia function and maintenance during development and adulthood. Perinatal absence of Dicer impaired proliferative expansion and DNA integrity of microglia and caused spontaneous hyper-activation. Microglial *Dicer* ablation in adulthood did not cause spontaneous activation of microglia in steady state, but resulted in microglial hyper-responsiveness to challenge and as a consequence, acute impairment of neuronal

circuitries. This differential impact of the Dicer deficiency highlights the prominent changes microglia undergo with time from the developing to the adult brain.

STAR★METHODS

Detailed methods are provided in the online version of this paper and include the following:

- KEY RESOURCES TABLE
- CONTACT FOR REAGENT AND RESOURCE SHARING
- EXPERIMENTAL MODEL AND SUBJECT DETAILS
  - ○ Transgenic Animal Models
- METHOD DETAILS
  - ○ Tamoxifen treatment
  - ○ BM chimera generation
  - ○ Histology
  - ○ 3D reconstruction of microglia
  - ○ Surgery and Two photon in vivo imaging
  - ○ Live imaging Analysis
  - ○ Microglia isolation procedures
  - ○ Flow cytometry
  - ○ EDU labeling
  - ○ Western blot
  - ○ Agilent microRNA microarray
  - ○ RNA-seq, Processing and Analysis
  - ○ qRT-PCR of miRNAs
  - ○ qRT-PCR of mRNAs
  - ○ Genomic DNA isolation
  - ○ Genotyping Dicer floxed and recombined alleles
  - ○ Electrophysiology on brain slices (LTP)
  - ○ Comet assay
  - ○ Motoric activity assay
  - ○ Bioinformatic prediction of miRNA target enrichment in a gene database
  - ○ Similarity measure between distinct lists of differentially expressed genes
- QUANTIFICATION AND STATISTICAL ANALYSIS
  - ○ Bioinformatic data analysis
- DATA AND SOFTWARE AVAILABILITY

SUPPLEMENTAL INFORMATION

Supplemental Information includes seven figures, two tables, and one document of guidelines for the R script-based hyper-geometric test used in this study and can be found with this article online at http://dx.doi.org/10.1016/j.immuni.2017.05.003.

AUTHOR CONTRIBUTIONS

D.V., A.M., and S.J. conceived the project; D.V. and S.J. designed the experiments; T.B., A.S., N.B., and S.B.-H. performed the experiments and analysis; Y.S.-H., L.C.-M., and H.K.-S. helped with RNa-seq profiling; S.Y. generated transgenic animals; E.D. and D.L. performed bioinformatic analysis and developed algorithms; M.F. performed intra-vital imaging analysis; N.M. performed electrophysiology analysis; E.H., M.P., and I.A. advised on experiments; D.V. and S.J. wrote the paper; and S.J. supervised the project.

REFERENCES

Agarwal, V., Bell, G.W., Nam, J.-W., and Bartel, D.P. (2015). Predicting effective microRNA target sites in mammalian mRNAs. eLife 4, 101.

Amit, I., Winter, D.R., and Jung, S. (2016). The role of the local environment and epigenetics in shaping macrophage identity and their effect on tissue homeostasis. Nat. Immunol. 17, 18–25.

Banerjee, S., Xie, N., Cui, H., Tan, Z., Yang, S., Icyuz, M., Abraham, E., and Liu, G. (2013). MicroRNA let-7c regulates macrophage polarization. J. Immunol. 190, 6542–6549.

Bartel, D.P. (2009). MicroRNAs: target recognition and regulatory functions. Cell 136, 215–233.

Bernstein, E., Kim, S.Y., Carmell, M.A., Murchison, E.P., Alcorn, H., Li, M.Z., Mills, A.A., Elledge, S.J., Anderson, K.V., and Hannon, G.J. (2003). Dicer is essential for mouse development. Nat. Genet. 35, 215–217.

Bertrand, J.Y., Jalil, A., Klaine, M., Jung, S., Cumano, A., and Godin, I. (2005). Three pathways to mature macrophages in the early mouse yolk sac. Blood 106, 3004–3011.

Bruttger, J., Karram, K., Wörtge, S., Regen, T., Marini, F., Hoppmann, N., Klein, M., Blank, T., Yona, S., Wolf, Y., et al. (2015). Genetic cell ablation reveals clusters of local self-renewing microglia in the mammalian central nervous system. Immunity 43, 92–106.

Butovsky, O., Siddiqui, S., Gabriely, G., Lanser, A.J., Dake, B., Murugaiyan, G., Doykan, C.E., Wu, P.M., Gali, R.R., Iyer, L.K., et al. (2012). Modulating inflammatory monocytes with a unique microRNA gene signature ameliorates murine ALS. J. Clin. Invest. 122, 3063–3087.

Butovsky, O., Jedrychowski, M.P., Moore, C.S., Cialic, R., Lanser, A.J., Gabriely, G., Koeglsperger, T., Dake, B., Wu, P.M., Doykan, C.E., et al. (2014). Identification of a unique TGF-β-dependent molecular and functional signature in microglia. Nat. Neurosci. 17, 131–143.

Buttgereit, A., Lelios, I., Yu, X., Vrohlings, M., Krakoski, N.R., Gautier, E.L., Nishinakamura, R., Becher, B., and Greter, M. (2016). Sall1 is a transcriptional regulator defining microglia identity and function. Nat. Immunol. 17, 1397–1406.

Cellier, M.F., Courville, P., and Campion, C. (2007). Nramp1 phagocyte intracellular metal withdrawal defense. Microbes Infect. 9, 1662–1670.

Cheloufi, S., Dos Santos, C.O., Chong, M.M., and Hannon, G.J. (2010). A dicer-independent miRNA biogenesis pathway that requires Ago catalysis. Nature 465, 584–589.

Davalos, D., Grutzendler, J., Yang, G., Kim, J.V., Zuo, Y., Jung, S., Littman, D.R., Dustin, M.L., and Gan, W.-B. (2005). ATP mediates rapid microglial response to local brain injury in vivo. Nat. Neurosci. 8, 752–758.

Dennis, G., Jr., Sherman, B.T., Hosack, D.A., Yang, J., Gao, W., Lane, H.C., and Lempicki, R.A. (2003). DAVID: Database for Annotation, Visualization, and Integrated Discovery. Genome Biol. 4, 3.

Francia, S., Michelini, F., Saxena, A., Tang, D., de Hoon, M., Anelli, V., Mione, M., Carninci, P., and d'Adda di Fagagna, F. (2012). Site-specific DICER and DROSHA RNA products control the DNA-damage response. Nature 488, 231–235.

Fuhrmann, M., Bittner, T., Jung, C.K.E., Burgold, S., Page, R.M., Mitteregger, G., Haass, C., LaFerla, F.M., Kretzschmar, H., and Herms, J. (2010). Microglial Cx3cr1 knockout prevents neuron loss in a mouse model of Alzheimer's disease. Nat. Neurosci. *13*, 411–413.

Gelfand, B.D., Wright, C.B., Kim, Y., Yasuma, T., Yasuma, R., Li, S., Fowler, B.J., Bastos-Carvalho, A., Kerur, N., Uittenbogaard, A., et al. (2015). Iron toxicity in the retina requires Alu RNA and the NLRP3 inflammasome. Cell Rep. *11*, 1686–1693.

Ginhoux, F., and Guilliams, M. (2016). Tissue-resident macrophage ontogeny and homeostasis. Immunity *44*, 439–449.

Ginhoux, F., Greter, M., Leboeuf, M., Nandi, S., See, P., Gokhan, S., Mehler, M.F., Conway, S.J., Ng, L.G., Stanley, E.R., et al. (2010). Fate mapping analysis reveals that adult microglia derive from primitive macrophages. Science *330*, 841–845.

Goldmann, T., Wieghofer, P., Müller, P.F., Wolf, Y., Varol, D., Yona, S., Brendecke, S.M., Kierdorf, K., Staszewski, O., Datta, M., et al. (2013). A new type of microglia gene targeting shows TAK1 to be pivotal in CNS autoimmune inflammation. Nat. Neurosci. *16*, 1618–1626.

Goldmann, T., Wieghofer, P., Jordão, M.J.C., Prutek, F., Hagemeyer, N., Frenzel, K., Amann, L., Staszewski, O., Kierdorf, K., Krueger, M., et al. (2016). Origin, fate and dynamics of macrophages at central nervous system interfaces. Nat. Immunol. *17*, 797–805.

Gosselin, D., Link, V.M., Romanoski, C.E., Fonseca, G.J., Eichenfield, D.Z., Spann, N.J., Stender, J.D., Chun, H.B., Garner, H., Geissmann, F., and Glass, C.K. (2014). Environment drives selection and function of enhancers controlling tissue-specific macrophage identities. Cell *159*, 1327–1340.

Guerreiro, R., and Hardy, J. (2013). TREM2 and neurodegenerative disease. N. Engl. J. Med. *369*, 1569–1570.

Guo, H., Ingolia, N.T., Weissman, J.S., and Bartel, D.P. (2010). Mammalian microRNAs predominantly act to decrease target mRNA levels. Nature *466*, 835–840.

Habbas, S., Santello, M., Becker, D., Stubbe, H., Zappia, G., Liaudet, N., Klaus, F.R., Kollias, G., Fontana, A., Pryce, C.R., et al. (2015). Neuroinflammatory TNFα impairs memory via astrocyte signaling. Cell *163*, 1730–1741.

Harfe, B.D., McManus, M.T., Mansfield, J.H., Hornstein, E., and Tabin, C.J. (2005). The RNaseIII enzyme Dicer is required for morphogenesis but not patterning of the vertebrate limb. Proc. Natl. Acad. Sci. USA *102*, 10898–10903.

Harry, G.J. (2013). Microglia during development and aging. Pharmacol. Ther. *139*, 313–326.

Heinz, S., Benner, C., Spann, N., Bertolino, E., Lin, Y.C., Laslo, P., Cheng, J.X., Murre, C., Singh, H., and Glass, C.K. (2010). Simple combinations of lineage-determining transcription factors prime cis-regulatory elements required for macrophage and B cell identities. Mol. Cell *38*, 576–589.

Huang, W., Sherman, B.T., and Lempicki, R.A. (2009). Bioinformatics enrichment tools: paths toward the comprehensive functional analysis of large gene lists. Nucleic Acids Res. *37*, 1–13.

Ihaka, R., and Gentleman, R. (1996). R: A Language for Data Analysis and Graphics. J. Comput. Graph. Stat. *5*, 299–314.

Iliopoulos, D., Hirsch, H.A., and Struhl, K. (2009). An epigenetic switch involving NF-kappaB, Lin28, Let-7 MicroRNA, and IL6 links inflammation to cell transformation. Cell *139*, 693–706.

Jaitin, D.A., Kenigsberg, E., Keren-Shaul, H., Elefant, N., Paul, F., Zaretsky, I., Mildner, A., Cohen, N., Jung, S., Tanay, A., and Amit, I. (2014). Massively parallel single-cell RNA-seq for marker-free decomposition of tissues into cell types. Science *343*, 776–779.

Jung, S., Aliberti, J., Graemmel, P., Sunshine, M.J., Kreutzberg, G.W., Sher, A., and Littman, D.R. (2000). Analysis of fractalkine receptor CX(3)CR1 function by targeted deletion and green fluorescent protein reporter gene insertion. Mol. Cell. Biol. *20*, 4106–4114.

Kaneko, H., Dridi, S., Tarallo, V., Gelfand, B.D., Fowler, B.J., Cho, W.G., Kleinman, M.E., Ponicsan, S.L., Hauswirth, W.W., Chiodo, V.A., et al. (2011). DICER1 deficit induces Alu RNA toxicity in age-related macular degeneration. Nature *471*, 325–330.

Kierdorf, K., Erny, D., Goldmann, T., Sander, V., Schulz, C., Perdiguero, E.G., Wieghofer, P., Heinrich, A., Riemke, P., Hölscher, C., et al. (2013). Microglia emerge from erythromyeloid precursors via Pu.1- and Irf8-dependent pathways. Nat. Neurosci. *16*, 273–280.

Kiermayer, C., Conrad, M., Schneider, M., Schmidt, J., and Brielmeier, M. (2007). Optimization of spatiotemporal gene inactivation in mouse heart by oral application of tamoxifen citrate. Genesis *45*, 11–16.

Kim, V.N., Han, J., and Siomi, M.C. (2009). Biogenesis of small RNAs in animals. Nat. Rev. Mol. Cell Biol. *10*, 126–139.

Koralov, S.B., Muljo, S.A., Galler, G.R., Krek, A., Chakraborty, T., Kanellopoulou, C., Jensen, K., Cobb, B.S., Merkenschlager, M., Rajewsky, N., and Rajewsky, K. (2008). Dicer ablation affects antibody diversity and cell survival in the B lymphocyte lineage. Cell *132*, 860–874.

Kuipers, H., Schnorfeil, F.M., Fehling, H.J., Bartels, H., and Brocker, T. (2010). Dicer-dependent microRNAs control maturation, function, and maintenance of Langerhans cells in vivo. J. Immunol. *185*, 400–409.

Lallemand, Y., Luria, V., Haffner-Krausz, R., and Lonai, P. (1998). Maternally expressed PGK-Cre transgene as a tool for early and uniform activation of the Cre site-specific recombinase. Transgenic Res. *7*, 105–112.

Lavin, Y., Winter, D., Blecher-Gonen, R., David, E., Keren-Shaul, H., Merad, M., Jung, S., and Amit, I. (2014). Tissue-resident macrophage enhancer landscapes are shaped by the local microenvironment. Cell *159*, 1312–1326.

Lawson, L.J., Perry, V.H., and Gordon, S. (1992). Turnover of resident microglia in the normal adult mouse brain. Neuroscience *48*, 405–415.

Love, M.I., Huber, W., and Anders, S. (2014). Moderated estimation of fold change and dispersion for RNA-seq data with DESeq2. Genome Biol. *15*, 550.

Maggio, N., and Segal, M. (2007). Striking variations in corticosteroid modulation of long-term potentiation along the septotemporal axis of the hippocampus. J. Neurosci. *27*, 5757–5765.

Maggio, N., Shavit-Stein, E., Dori, A., Blatt, I., and Chapman, J. (2013). Prolonged systemic inflammation persistently modifies synaptic plasticity in the hippocampus: modulation by the stress hormones. Front. Mol. Neurosci. *6*, 46.

Mancino, A., Habbeddine, M., Johnson, E., Luron, L., Bebien, M., Memet, S., Fong, C., Bajénoff, M., Wu, X., Karin, M., et al. (2013). I kappa B kinase alpha (IKKα) activity is required for functional maturation of dendritic cells and acquired immunity to infection. EMBO J. *32*, 816–828.

Mass, E., Ballesteros, I., Farlik, M., Halbritter, F., Günther, P., Crozet, L., Jacome-Galarza, C.E., Händler, K., Klughammer, J., Kobayashi, Y., et al. (2016). Specification of tissue-resident macrophages during organogenesis. Science *353*, 1–22.

Matcovitch-Natan, O., Winter, D.R., Giladi, A., Vargas Aguilar, S., Spinrad, A., Sarrazin, S., Ben-Yehuda, H., David, E., Zelada González, F., Perrin, P., et al. (2016). Microglia development follows a stepwise program to regulate brain homeostasis. Science *353*, aad8670.

McKinnon, P.J. (2013). Maintaining genome stability in the nervous system. Nat. Neurosci. *16*, 1523–1529.

Mildner, A., Schmidt, H., Nitsche, M., Merkler, D., Hanisch, U.-K., Mack, M., Heikenwalder, M., Brück, W., Priller, J., and Prinz, M. (2007). Microglia in the adult brain arise from Ly-6ChiCCR2+ monocytes only under defined host conditions. Nat. Neurosci. *10*, 1544–1553.

Nimmerjahn, A., Kirchhoff, F., and Helmchen, F. (2005). Resting microglial cells are highly dynamic surveillants of brain parenchyma in vivo. Science *308*, 1314–1318.

O'Connell, R.M., Rao, D.S., and Baltimore, D. (2012). microRNA regulation of inflammatory responses. Annu. Rev. Immunol. *30*, 295–312.

Olive, P.L., and Banáth, J.P. (2006). The comet assay: a method to measure DNA damage in individual cells. Nat. Protoc. *1*, 23–29.

Orłowski, D., Sołtys, Z., and Janeczko, K. (2003). Morphological development of microglia in the postnatal rat brain. A quantitative study. Int. J. Dev. Neurosci. *21*, 445–450.

Paolicelli, R.C., Bolasco, G., Pagani, F., Maggi, L., Scianni, M., Panzanelli, P., Giustetto, M., Ferreira, T.A., Guiducci, E., Dumas, L., et al. (2011). Synaptic

pruning by microglia is necessary for normal brain development. Science 333, 1456–1458.

Poliani, P.L., Wang, Y., Fontana, E., Robinette, M.L., Yamanishi, Y., Gilfillan, S., and Colonna, M. (2015). TREM2 sustains microglial expansion during aging and response to demyelination. J. Clin. Invest. 125, 2161–2170.

Prinz, M., and Priller, J. (2014). Microglia and brain macrophages in the molecular age: from origin to neuropsychiatric disease. Nat. Rev. Neurosci. 15, 300–312.

Rademakers, R., Baker, M., Nicholson, A.M., Rutherford, N.J., Finch, N., Soto-Ortolaza, A., Lash, J., Wider, C., Wojtas, A., DeJesus-Hernandez, M., et al. (2011). Mutations in the colony stimulating factor 1 receptor (CSF1R) gene cause hereditary diffuse leukoencephalopathy with spheroids. Nat. Genet. 44, 200–205.

Riazi, K., Galic, M.A., Kentner, A.C., Reid, A.Y., Sharkey, K.A., and Pittman, Q.J. (2015). Microglia-dependent alteration of glutamatergic synaptic transmission and plasticity in the hippocampus during peripheral inflammation. J. Neurosci. 35, 4942–4952.

Saba, R., Gushue, S., Huzarewich, R.L.C.H., Manguiat, K., Medina, S., Robertson, C., and Booth, S.A. (2012). MicroRNA 146a (miR-146a) is overexpressed during prion disease and modulates the innate immune response and the microglial activation state. PLoS ONE 7, e30832–e16.

Schaefer, A., O'Carroll, D., Tan, C.L., Hillman, D., Sugimori, M., Llinas, R., and Greengard, P. (2007). Cerebellar neurodegeneration in the absence of microRNAs. J. Exp. Med. 204, 1553–1558.

Schafer, D.P., Lehrman, E.K., Kautzman, A.G., Koyama, R., Mardinly, A.R., Yamasaki, R., Ransohoff, R.M., Greenberg, M.E., Barres, B.A., and Stevens, B. (2012). Microglia sculpt postnatal neural circuits in an activity and complement-dependent manner. Neuron 74, 691–705.

Schmiedel, J.M., Klemm, S.L., Zheng, Y., Sahay, A., Blüthgen, N., Marks, D.S., and van Oudenaarden, A. (2015). Gene expression. MicroRNA control of protein expression noise. Science 348, 128–132.

Squarzoni, P., Oller, G., Hoeffel, G., Pont-Lezica, L., Rostaing, P., Low, D., Bessis, A., Ginhoux, F., and Garel, S. (2014). Microglia modulate wiring of the embryonic forebrain. Cell Rep. 8, 1271–1279.

Srinivas, S., Watanabe, T., Lin, C.S., William, C.M., Tanabe, Y., Jessell, T.M., and Costantini, F. (2001). Cre reporter strains produced by targeted insertion of EYFP and ECFP into the ROSA26 locus. BMC Dev. Biol. 1, 4.

Strehl, A., Lenz, M., Itsekson-Hayosh, Z., Becker, D., Chapman, J., Deller, T., Maggio, N., and Vlachos, A. (2014). Systemic inflammation is associated with a reduction in Synaptopodin expression in the mouse hippocampus. Exp. Neurol. 261, 230–235.

Subramanian, A., Tamayo, P., Mootha, V.K., Mukherjee, S., Ebert, B.L., Gillette, M.A., Paulovich, A., Pomeroy, S.L., Golub, T.R., Lander, E.S., and Mesirov, J.P. (2005). Gene set enrichment analysis: a knowledge-based approach for interpreting genome-wide expression profiles. Proc. Natl. Acad. Sci. USA 102, 15545–15550.

Swahari, V., Nakamura, A., Baran-Gale, J., Garcia, I., Crowther, A.J., Sons, R., Gershon, T.R., Hammond, S., Sethupathy, P., and Deshmukh, M. (2016). Essential function of Dicer in resolving DNA damage in the rapidly dividing cells of the developing and malignant cerebellum. Cell Rep. 14, 216–224.

Taganov, K.D., Boldin, M.P., Chang, K.-J., and Baltimore, D. (2006). NF-kappaB-dependent induction of microRNA miR-146, an inhibitor targeted to signaling proteins of innate immune responses. Proc. Natl. Acad. Sci. USA 103, 12481–12486.

Tao, J., Wu, H., Lin, Q., Wei, W., Lu, X.H., Cantle, J.P., Ao, Y., Olsen, R.W., Yang, X.W., Mody, I., et al. (2011). Deletion of astroglial Dicer causes non-cell-autonomous neuronal dysfunction and degeneration. J. Neurosci. 31, 8306–8319.

Trapnell, C., Pachter, L., and Salzberg, S.L. (2009). TopHat: discovering splice junctions with RNA-Seq. Bioinformatics 25, 1105–1111.

Turner, M.L., Schnorfeil, F.M., and Brocker, T. (2011). MicroRNAs regulate dendritic cell differentiation and function. J. Immunol. 187, 3911–3917.

Varol, C., Mildner, A., and Jung, S. (2015). Macrophages: development and tissue specialization. Annu. Rev. Immunol. 33, 643–675.

Vereker, E., Campbell, V., Roche, E., McEntee, E., and Lynch, M.A. (2000). Lipopolysaccharide inhibits long term potentiation in the rat dentate gyrus by activating caspase-1. J. Biol. Chem. 275, 26252–26258.

Wang, Y., Cella, M., Mallinson, K., Ulrich, J.D., Young, K.L., Robinette, M.L., Gilfillan, S., Krishnan, G.M., Sudhakar, S., Zinselmeyer, B.H., et al. (2015). TREM2 lipid sensing sustains the microglial response in an Alzheimer's disease model. Cell 160, 1061–1071.

Wei, W., Ba, Z., Gao, M., Wu, Y., Ma, Y., Amiard, S., White, C.I., Rendtlew Danielsen, J.M., Yang, Y.-G., and Qi, Y. (2012). A role for small RNAs in DNA double-strand break repair. Cell 149, 101–112.

Wolf, Y., Boura-Halfon, S., Cortese, N., Haimon, Z., Sar Shalom, H., Kuperman, Y., Kalchenko, V., Brandis, A., David, E., Segal-Hayoun, Y., et al. (2017). Brown-adipose-tissue macrophages control tissue innervation and homeostatic energy expenditure. Nat. Immunol. 18, 665–674.

Yona, S., Kim, K.-W., Wolf, Y., Mildner, A., Varol, D., Breker, M., Strauss-Ayali, D., Viukov, S., Guilliams, M., Misharin, A., et al. (2013). Fate mapping reveals origins and dynamics of monocytes and tissue macrophages under homeostasis. Immunity 38, 79–91.

Zhang, L., Dong, L.-Y., Li, Y.-J., Hong, Z., and Wei, W.-S. (2012). The microRNA miR-181c controls microglia-mediated neuronal apoptosis by suppressing tumor necrosis factor. J. Neuroinflammation 9, 211–226.

Zhou, B.B., and Elledge, S.J. (2000). The DNA damage response: putting checkpoints in perspective. Nature 408, 433–439.

STAR★METHODS

KEY RESOURCES TABLE

REAGENT or RESOURCE	SOURCE	IDENTIFIER
Antibodies		
Anti-CD11b PE-Cy7 (clone M1/70)	Biolegend	Cat#: 101215, RRID: AB_312798
Anti-CD11b FITC (Clone M1/70)	Biolegend	Cat#: 101205, RRID: AB_312788
Anti-CD45 APC (Clone 30-F11)	Biolegend	Cat#: 103112, RRID: AB_312976
Anti-CD45.1 APC (Clone A20)	Biolegend	Cat#: 110714, RRID: AB_313503
Anti-CD45.2, PB (Clone 104)	Biolegend	Cat#: 109820, RRID: AB_492872
Anti-Ly6C, PerCP-cy5.5 (Clone AL-21)	Biolegend	Cat#:128012, RRID: AB_1659241
Anti-LY6G, PE labeled (Clone 1A8)	Biolegend	Cat#: 127607, RRID:AB_1186104
Anti-LY6G, PB labeled (Clone 1A8)	Biolegend	Cat#: 127612, RRID:AB_2251161
Anti-I-Ab (MHCII), PE-Cy7 (Clone AF6-120.1)	Biolegend	Cat#:116420, RRID: AB_10575296
Anti-CD86, PE (Clone GL1)	Biolegend	Cat#:105008, RRID: AB_313151
Anti-CD64, PE (Clone X54-5/7.1)	Biolegend	Cat#: 139304, RRID: AB_10612740
Anti-CD11c, APC (Clone N418)	Biolegend	Cat#: 117310, RRID: AB_313779
Anti-CD40, PE (3/23)	Biolegend	Cat#:124609, RRID: AB_1134084
Anti-CD34, BV 421 (Clone MEC-14.7)	Biolegend	Cat#:119321, RRID:AB_10900980
Anti-CD61, Alexa fluor 488 (Clone 2C9.G2 (HMβ3-1))	Biolegend	Cat#:104311, RRID: AB_2128907
Anti-TCR$\gamma\delta$, APC (Clone GL3)	Biolegend	Cat#: 118116, RRID: AB_1731813
Anti-Il1b, PE (flow-cytometry, Clone NJTEN3)	Thermo Fisher (eBioscience)	Cat#:12-7114-82, RRID: AB_10732630
Goat polyclonal anti mouse Il1b (western blot)	R&D	Cat# AF-401-NA, RRID: AB_416684
Anti-Ki67, PE (Clone SolA15)	Thermo Fisher (eBioscience)	Cat#: 12-5698-82, RRID: AB_11150954
Anti-F4/80, PE (Clone Cl:A3-1)	Serotec	Cat#: MCA497PE, RRID: AB_322048
Anti-CD68 (Clone FA-11)	Biolegend	Cat#: 137001, RRID: AB_2044003
Rabbit polyclonal anti Iba1	Wako	Cat#: 016-20001, RRID: AB_839506
Cy3-AffiniPure Donkey Anti-Rabbit IgG (H+L)	Jackson Immuno-research	Cat#: 711-165-152, RRID: AB_2307443
Cy2-AffiniPure Donkey Anti-Rabbit IgG (H+L)	Jackson Immuno-research	Cat#: 711-225-152, RRID: AB_2340612
Alexa Fluor 568 donkey anti rabbit IgG (H+L)	Thermo Scientiffic (Life Technologies)	Cat#: A10042, RRID: AB_2534017
Chemicals, Peptides, and Recombinanat Proteins		
Agencourt AMPure XP	Beckman Coulter	Cat# A63881
Exonuclease I	New England Biolabs	Cat# M0293L
NEBNext mRNA Second Strand Synthesis Module	New England Biolabs	Cat# e6111L
RNA Fragmentation Reagents	Thermo Fisher	Cat# AM8740
Turbo DNase I	Thermo Fisher	Cat# AM2239
T4 RNA Ligase 1	New England Biolabs	Cat# M0204L
HiScribe T7 High Yield RNA Synthesis Kit	New England Biolabs	Cat# E2040
Kapa hifi PCR Kits	Kapabiosystems	Cat# KK2602
AffinityScript Multiple Temperature Reverse Transcriptase	Agilent	Cat# 600109
PowerUp SYBR Green Master Mix	Thermo Fisher	Cat# A25777
5 ethynyl-29-deoxyuridine (EDU)	Carbosynth	Cat#:NE08701
PB labeled AnnexinV	Biolegend	Cat#: 640918
Annexin V Binding Buffer	Biolegend	Cat#: 422201
7AAD	BD	Cat#: 559925
DAPI	Biolegend	Cat#: 422801
Tamoxifen	Sigma	Cat#: T5648
LPS from E.Coli 0111:B4	Sigma	Cat#: L4130

(Continued on next page)

REAGENT or RESOURCE	SOURCE	IDENTIFIER
Polyinosinic–polycytidylic acid sodium salt (Poly I/C)	Sigma	Cat#: P1530
Para-Form-Aldehyde (PFA), prilled	Sigma	Cat#: 441244
TBE buffer (For Comet assay)	Biological industries	Cat#: 01-871-1A
SYBR green I dye 10,000X (For comet assay)	Thermo Fisher	*Cat#:S11494*
NP-40 (for western blot)	Abcam	Cat#:ab142227
Sodium deoxycholate (for western blot)	Sigma	Cat#: D6750
Sodium pyrophosphate (for western blot)	Sigma	Cat#: P8010
beta-glycerophosphate (for western blot)	Sigma	Cat#: G9422
Citrate buffer, 10X, PH = 6 (for Histology, Ag retriever)	Sigma	Cat# C9999
Dexamethasone (used during in-vivo imaging of microglia)	Sigma	Cat#: D4902
Ketamin 50 mg/ml (10ml vial)	VetMarket (Israel)	Cat#: 102517
Xylasine 10% (25 ml vial)	VetMarket (Israel)	Cat#: 102656
Ciproxin 0.2 g/ml	Bayer Israel LTD	Cat#: 28863
Critical Commercial Assays		
Fixation/permeabilization solution kit	BD	Cat#: 554714
Click it EDU detection kit	Thermo Fisher (Invitrogen)	Cat#: C10340
miRNeasy micro kit	QIAGEN	Cat#: 217084
Miscript reverse transcription kit (for total RNA incl. miRNA)	QIAGEN	Cat#: 218160
Dynabeads mRNA DIRECT Purification Kit	Thermo Fisher scientific	*Cat#: 61012*
AffinityScript Multiple Temperature Reverse Transcriptase (for mRNA)	Agilent	Cat#: 600109
Dneasy Blood and tissue kit	QIAGEN	Cat#: 69506
Comet assay	Trevigen	Cat#: 4250-050-K
Deposited Data		
Raw and analyzed data	GEO	GSE98144 (including GSE98142 for RNA-seq data and GSE98143 for Agilent microarray)
Experimental Models: Mouse strains		
C57BL/6 (CD45.2)	Harlan	C57BL/6 RRID: IMSR_JAX000664
B6.SJL (CD45.1)	Jackson	B6.SJL-*Ptprc*[a] *Pepc*[b]/BoyJ RRID: IMSR_JAX002014
Cx3cr1[gfp/+]	Jackson (Jung et al., 2000)	B6.129P-Cx3cr1tm1Litt/J RRID: IMSR_JAX005582
Cx3cr1[Cre]	Jackson (Yona et al., 2013)	B6J.B6N(Cg)-Cx3cr1tm1.1(cre)Jung/J RRID: IMSR_JAX025524
Cx3cr1[CreER]	Jackson (Yona et al., 2013)	B6.129P2(C)-Cx3cr1tm2.1(cre/ERT2)Jung/J RRID: IMSR_JAX020940
Dicer^{fl/fl}	Jackson (Harfe et al., 2005)	B6.Cg-*Dicer1tm1Bdh*/J RRID: IMSR_JAX006366
Rosa-26-YFP	Jackson (Srinivas et al., 2001)	B6.129X1-*Gt(ROSA)26Sortm1(EYFP)Cos*/J RRID: IMSR_JAX006148
Pgk[Cre]	Jackson (Lallemand et al., 1998)	B6.C-Tg(Pgk1-cre)1Lni/CrsJ RRID: IMSR_JAX020811
Oligonucleotides		
Primers for qPCR of transcripts, see Table S2	This paper	N/A
Dicer WT/fl allele FW: ACAGTGACGGTCCAAA GTAAAG	Modified from Harfe et al., 2005	N/A
Dicer WT/fl allele Rev: CATGACTCTTCAACTCAAACT	Harfe et al., 2005	N/A

Continued

REAGENT or RESOURCE	SOURCE	IDENTIFIER
Dicer recombined fl allele Rev: CCTGAGTAAGGCAAG TCATTC	Harfe et al., 2005	N/A
MARS-Seq barcoded RT primer: CGATTGAGG CCGGTAATACGACTCACTATAGGGGCGACGT GTGCTCTTCCGATCTXXXXXXNNNNTTTTTT TTTTTTTTTTTTTTN, where XXXXXX is the cell barcode and NNNN is the RMT	Jaitin et al., 2014	N/A
MARS-Seq ligation primer: AGATCGGAAGAGCG TCGTGTAG, modified with a phosphate group at 5′ and a C3 spacer (blocker) at the 3′	Jaitin et al., 2014	N/A
MARS-Seq 2nd RT primer: TCTAGCCTTCT CGCAGCACATC	Jaitin et al., 2014	N/A
MARS-Seq P5_Rd1: PCR forward, AATGATACGG CGACCACCGAGATCTACACTCTTTCCCTACA CGACGCTCTTCCGATCT	Jaitin et al., 2014	N/A
MARS-Seq P7_Rd2: PCR reverse, CAAGCAGAAG ACGGCATACGAGATGTGACTGGAGTTCAGACGT GTGCTCTTCCGATCT	Jaitin et al., 2014	N/A
Software and Algorithms		
TargetscanMouse 7.1 (Used for downloading the list of genes with conserved and non-conserved sites in UTRs corresponding to conserved miRNA families)	Agarwal et al., 2015 (MIT)	http://www.targetscan.org/cgi-bin/ targetscan/data_download.cgi?db= mmu_71 RRID: SCR_002014
Gene Set Enrichment Analysis (GSEA)	Subramanian et al., 2005 (Broad Institute)	http://software.broadinstitute.org/gsea/ index.jsp RRID: SCR_003199
R package	Ihaka and Gentleman, 1996 (University of Aukland)	https://stat.ethz.ch/R-manual/R-devel/ library/stats/html/Hypergeometric.html
A hypergeometric R package based statistical analysis; measuring enrichment of miR targets in a gene expression dataset.	This paper	https://bbcunit.atlassian.net/wiki/ display/BP/miR+target+enrichment+ for+mouse
Partek genomic suite software, version 6.6	Partek Inc., St. Louis	http://www.partek.com/pgs RRID: SCR_011860
Deseq-2 R package	Love et al., 2014 (Bioconductor)	https://bioconductor.org/packages/ release/bioc/html/DESeq2.html RRID: SCR_000154
HOMER (Hypergeometric Optimization of Motif EnRichment)	Heinz et al., 2010 (The Integrative Genomics and bioinformatics core, The Salk Institute)	http://homer.ucsd.edu/homer/index.html RRID: SCR_010881
MATLAB	MathWorks	https://www.mathworks.com/ downloads/?requestedDomain=www. mathworks.com RRID: SCR_001622
GeneE	Broad Institute	https://software.broadinstitute.org/ GENE-E/download.html
Ingenuity	QIAGEN bioinformatics	https://www.qiagenbioinformatics.com/ products/ingenuity-pathway-analysis/ RRID: SCR:_008653
DAVID	Huang et al., 2009 (National Institute of Allergy and Infectious Diseases, NIH)	https://david.ncifcrf.gov/summary.jsp RRID: SCR:_003033
IMARIS software (3D microglia reconstruction)	Bitplane	RRID: SCR:_007370
Spike 2 software (LTP electrophysiology analysis)	Cambridge Electronic Design	RRID: SCR:_000903
GraphPad Prism 6	GraphPad Software	RRID: SCR:_002798
FlowJo 8.7	TreeStar; FlowJo	RRID: SCR:_008520

CONTACT FOR REAGENT AND RESOURCE SHARING

Further information and requests for reagents may be directed to and will be fulfilled by Lead Contact, Prof. Steffen Jung (s.jung@weizmann.ac.il).

EXPERIMENTAL MODEL AND SUBJECT DETAILS

Both male and female mice were used for all experiments. Mice aged 6-30 weeks old were used for adult microglia experiments. For the developing microglia studies, E14 embryonic stage and newborn (P0) microglia were used.

Conditional CreER-loxP and Cre-LoxP systems were used in order to either induce Dicer deletion in adult microglia ($Cx3cr1^{CreER}$:$Dicer^{fl/-}$), requiring injections with tamoxifen (see tamoxifen treatment under method details section) or for the constitutive Dicer loss in microglia starting at embryonic development ($Cx3cr1^{Cre}$:$Dicer^{fl/fl}$). BM chimeras were used to examine microglia radio-sensitivity in response to *Dicer* loss (see Figure 7C, D, Figure S6B), (see BM chimeras generation under methods details section).

Mice were maintained on a 12 hr light/dark cycle, and food and water was provided ad libitum. All animals were on C57BL/6JOlaHsd background, maintained in specific pathogen-free (SPF) conditions and handled according to protocols approved by the Weizmann Institute Animal Care Committee (IACUC), as per international guidelines. The mouse strains were either purchased from Envigo (Harlan) (CD45.2), Jackson Laboratory and bred in the Weizmann Institute of Science (CD45.1, $Cx3cr1^{gfp/+}$, $Dicer^{fl/fl}$, *Rosa26*-YFP, Pgk^{Cre}) or generated and bred at the Weizmann Institute of Science ($Cx3cr1^{Cre}$, $Cx3cr1^{CreER}$).

Transgenic Animal Models

The conditional $Cx3cr1^{Cre}$:$Dicer^{fl/fl}$ mouse line was generated by breeding $Cx3cr1^{Cre}$ and $Dicer^{fl/fl}$ mice. The conditional and inducible $Cx3cr1^{CreER}$:$Dicer^{fl/-}$ and control ($Cx3cr1^{CreER}$:$Dicer^{+/-}$) mouse lines were generated by breeding $Dicer^{fl/fl}$ with Pgk^{Cre} mice, yielding $Dicer^{fl/-}$ mice which were then bred with $Cx3cr1^{CreER}$ animals. Generation and genotyping of $Cx3cr1^{Cre}$ and $Cx3cr1^{CreER}$ driver lines (Yona et al., 2013), Pgk^{Cre} driver line (Lallemand et al., 1998), $Dicer^{fl/fl}$ conditional mutant line (Harfe et al., 2005), $Cx3cr1^{gfp/+}$ reporter line (Jung et al., 2000) and R26-YFP reporter line (Srinivas et al., 2001) have been previously described.

METHOD DETAILS

Tamoxifen treatment

To induce gene recombination in CreER transgenic mice, tamoxifen (TAM) was dissolved in warm corn oil (Sigma) and administered orally via gavage for five consecutive times (Kiermayer et al., 2007). All animals were TAM-treated first at four weeks of age. Each oral application was of 10 mg at a concentration of 10 mg/100 μl. Mice were examined at least six weeks following treatment, unless indicated differently. For LPS treatment, mice were either injected intraperitoneally (*i.p.*) with a single dose of LPS [1 mg/kg; $\geq$ 500,000 (endotoxin units)/mg; *E. coli* 0111:B4; Sigma], the same volume of vehicle solution (PBS), or non-treated. For poly I:C treatment, mice were either injected i.p with a single dose of poly I:C [20 mg/kg], the same volume of vehicle solution (PBS), or non-treated.

BM chimera generation

BM chimeras were lethally irradiated (950 rad) and reconstituted the following day via i.v. injection of 5×10^6 donor whole BM cells per mouse; mice were next supplemented with Ciproxin 1:100 in their drinking water (Bayer Israel LTD) for 10 days. Chimera analysis was performed six weeks following the BM transfer, unless indicated differently (see Figure S6B).

Histology

Following paraformaldehyde (PFA) fixation (48 hr in 4°C), brain and spinal cord (SC) were taken for frozen and paraffin sections, respectively. For frozen sections, following incubation in PFA, tissues were equilibrated with 30% (wt/ vol) sucrose solution for 48 hr. Subsequently, samples were snap frozen in O.C.T (Tissue-Tek) by isopentane (Sigma) previously cooled with liquid nitrogen, and sectioned with a cryostat into 12 μm thick sections. Sections were stained with Iba1 (Wako, 1:150), CD68 (Biolegend, clone FA-11, 1:100) and Dapi (biolegend).

Primary Ab was then followed by 2nd Ab labeling, using Cy3-AffiniPure Donkey Anti-Rabbit IgG (H+L) (Jackson Immuno-research) or Alexa Fluor 568 donkey anti rabbit IgG (H+L) (Thermo Scientiffic (Life Technologies) for anti-Iba1 detection and with Cy2-AffiniPure Donkey Anti-rat IgG (H+L) (Jackson Immuno-research) for anti-CD68 detection.

For paraffin sections, following incubation in PFA, tissues were embedded in paraffin, serially sectioned and stained after antigen retrieval (Citrate buffer PH = 6, Sigma) with Iba1.

3D reconstruction of microglia

30-μm parasagittal cryosections from adult brain tissue were stained with anti-Iba1 (Wako) for 48 hr (dilution 1:500 at 4°C), followed by Alexa Fluor 568–conjugated secondary antibody (Life technologies), which was added at a dilution of 1:500 overnight at 4°C. Nuclei were counterstained with DAPI. Imaging was performed on an Olympus Fluoview 1000 confocal laser scanning microscope (Olympus) using a 20Å~0.95 NA objective. Z stacks performed with 1.14-mm steps in z direction, 1,024 Å~1,024 pixel resolution were recorded and analyzed using IMARIS software (Bitplane). Three to four cortical cells were reconstructed per analyzed mouse.

Surgery and Two photon in vivo imaging

A cranial window over the right cortical hemisphere was installed as previously described (Fuhrmann et al., 2010). Mice were anaesthetized with an intraperitoneal (*i.p.*) injection of ketamine/xylazin (0.13/0.01 mg/g body weight). Additionally, dexamethasone (0.02 ml at 4 mg/ml) was *i.p.* injected immediately before surgery to prevent swelling of the brain. A small incision was made to the skin over the right part of the skull. The skull was exposed and a circular piece of the skull (4 mm diameter) was removed using a dental drill (Schick-Technikmaster C1; Pluradent, Offenbach, Germany). A sterilized circular glass coverslip (4 mm diameter) was inserted into the hole and fixed using dental acrylic (Cyano-Veneer fast; Heinrich Schein Dental Depot, Munich, Germany). Next to the cranial window a small metal bar was glued containing a winding for fixation of the mouse in a stereotactic frame under the microscope. After surgery, mice were placed in the custom made stereotactic frame under the microscope (TrimScope II, LaVision Biotech, Germany) and supported by a heating plate to maintain the body temperature at 37°C. A 16X NA0.8 water immersion objective with a working distance of 3 mm (Nikon, Germany) was used to acquire images in vivo. YFP-fluorescent microglia were excited with a two-photon laser (Cameleon Ultra II, Coherent) at a wavelength of 920 nm with a maximum output power of 50mW to prevent photo damage. YFP emission was filtered with a bandpass filter (535-580 nm) and detected with highly sensitive gallium arsenide phosphide (GaAsP)-detector. Image stacks (400 × 400 × 300 μm) with a pixel size of 0.39 μm/pixel and a z-spacing of 3 μm were acquired every 5 min for a period of 40 min. At the end of the experiment, mice were sacrificed and the brains were removed for further processing.

Live imaging Analysis

The acquired z stacks were median filtered and average intensity projections were performed of 30 μm spanning stacks in z-dimension. The average intensity projected time-series were registered using the TurboReg plugin in FIJI (ImageJ). Two images of subsequent time-points were overlaid and the precursor images were pseudo-colored in green and the successor images in magenta. In these pseudo-colored images we measured the area of gained (green) and lost (magenta) microglial processes. The turnover rate (TOR) of microglial processes was calculated as the sum area of gained and lost processes, divided by the whole area occupied by the microglia cell in percent.

Microglia isolation procedures

For isolation of adult microglia, prior to tissue collection, mice were perfused with phosphate buffered saline (PBS) via the heart left ventricle. Brain and spinal cord were dissected, crudely homogenized by pipetting and incubated for 15 min at 37°C in a 1 ml HBSS solution containing 2% BSA, 1 mg/ml Collagenase D (Sigma) and 1 mg/ml DNase1 (Sigma). Next the homogenate was filtered through a 100 μm mesh, washed with cold PBS−/− and centrifuged at 1400 RPM, at 4°C, for 5 min. For the enrichment of microglia, the cell pellet was re-suspended with a 40% percoll solution and centrifuged at 2200 RPM, no acceleration and breaks, at 22°C for 20 min. Next, the cell pellet was taken for antibody (Ab) labeling and flow-cytometry analysis. For isolation of embryonic and newborn microglia, brain was gently pulled out and separated from the meninges; next the brain was grossly dissected and homogenized using gentleMACS tubes (Miltenyi, Bergisch Gladbach). For the enrichment of microglia, cell pellets were resuspended in a 40%/80% percoll solution and centrifuged at 2200 RPM, no acceleration and breaks, 22°C for 20 min. The gradient interphase was collected, washed with cold PBS (1:10 ratio) and centrifuged at 1400 RPM, at 4°C, for 5 min. Next, the cell pellet was taken for Ab labeling and flow-cytometry analysis.

Flow cytometry

Cells were stained with primary antibodies directed against CD11b (clone M1/70, PE-Cy7 and FITC labeled), CD45 (clone 30-F11), CD45.1 (clone A20), CD45.2 (clone 104), Ly6C (clone AL-21), LY6G (clone 1A8, PE labeled and PB labeled), MHC class II (clone 2G9), CD86 (clone GL-1), CD64 (clone X54-5/7.1) F4/80 (clone Cl:A3-1) CD11c (clone N418), CD40 (clone HM40-3), CD34 (clone MEC-14.7), CD61 (clone 2C9.G2 (HMβ3-1)), TCRγδ (clone GL3) and a labeled AnnexinV molecule - all Biolegend, San Diego, CA, USA. In addition we used primary antibodies directed against Il1b (Clone NJTEN3, eBioscience (Thermo scientific), Ki67 (clone SolA15, Thermo Scientific (eBioscience)), and 7AAD (BD, Erembodegem, Belgium). Following incubation with the surface Abs at 4°C for 15 min, cells were washed and analyzed using a FACSFortessa or for sorting with a FACSAriaIII (BD, Erembodegem, Belgium) flow cytometer. In the case of Ki67, following surface staining, cells were fixed and permeabilized (FixPerm kit, BD) for the intracellular labeling of Ki67. Viable cells were gated by forward and side scatter pattern. Data were acquired with FACSdiva software (Becton Dickinson). Post-acquisition analysis was performed using FlowJo software (Tree Star, FlowJo LLC; Ashland, Oregon).

EDU labeling

In order to measure P0 (newborn) microglia proliferation, 1.5 mg (50mg/Kg) of a thymidine analog, 5 ethynyl-29-deoxyuridine (EdU) (Invitrogen) diluted in 300 μl PBS supplemented with 1:500 DMSO was *i.p* injected twice to the pregnant mother at E19 with a three hours interval between injections. At P0 (usually E20) the brains of newborn mice were dissected and homogenized using the gentle MACS dispomix tubes (Miltenyi, Bergisch Gladbach). Next, brain cell suspension was enriched with a percoll gradient and stained with surface markers as described above. Following surface labeling, cells were fixed and permeabilized, followed by a chemical labeling of the incorporated EdU using the EdU staining kit according to manufacturer's instructions (Invitrogen).

Western blot
Tissues were extracted in RIPA buffer (20 mM Tris-HCl (pH 7.5), 150 mM NaCl, 1mM Na2EDTA, 1mM EGTA, 1% NP-40, 1% sodium deoxycholate, 2.5 mM sodium pyrophosphate, 1mM beta-glycerophosphate, 10mM NaF). Samples were separated by SDS-PAGE and immunoblotted using antibodies to IL1β (1:1000, R&D) and Vincullin (1:250, hybridoma).

Agilent microRNA microarray
Total RNA from freshly sorted microglia, colonic macrophages, and liver macrophages (KCs) was extracted using the miRNeasy micro Kit (QIAGEN). RNA purity was assessed with a BioAnalyzer 2100 (Agilent Technologies). Expression levels of miRNAs were assayed by Agilent miRNA microarrays (Release 12.0 and 15.0), according to the manufacturer's protocols. Then, 100 ng of total RNA per sample (duplicates for each cell population from independent sorts) was labeled and hybridized according to the manufacturer's instructions. For K-Means clustering with Pearson correlation, only miRNAs with a $\geq$ 2-fold differential expression in at least one comparison were used. As a target prediction algorithm, TargetScanMouse 7.1 was applied.

Bioinformatic analysis (raw intensity, signal normalization and calculation of fold change and statistically significant difference between groups) was performed with Partek Genomics Suite 6.6 software (http://www.partek.com/pgs).

Heatmaps graphics was performed with GeneE software (Broad Institute, https://software.broadinstitute.org/GENE-E/download.html).

RNA-seq, Processing and Analysis
For RNA-seq 30,000 microglia cells per brain were sorted by FACS directly into a 1.7 ml LoBind micro tubes (Eppendorff) containing 50 μl lysis buffer (RNase-free H$_2$O, 0.2% Triton-X (Roth) and 0.4 U/μl RNasin (Promega). Next, the tube was centrifuged, snap frozen on dry ice and stored at $-80°$C. mRNA was captured with Dynabeads® mRNA DIRECT Purification Kit (Thermo Fisher) according to manufacturer's guidelines. We used a derivation of MARS-seq (Jaitin et al., 2014) for the generation of RNA-Seq libraries. RNA-Seq libraries were sequenced using Illumina NextSeq-500, raw reads were mapped to the genome (NCBI37/mm9) using hisat (version 0.1.6) and only reads with unique mapping were considered for further analysis. Gene expression levels were calculated using the HOMER software package (analyzeRepeats.pl rna mm9 -d < tagDir > -count exons -condenseGenes -strand + -raw) (Heinz et al., 2010). RNA-seq reads were aligned to the mouse reference genome (NCBI 37, mm9) using TopHat v2.0.13 with default parameters (Trapnell et al., 2009). Duplicate reads were filtered if they aligned to the same base and had identical UMIs. Normalization and differential expression analysis was done using the DESeq2 R-package (Bioconductor, https://bioconductor.org/packages/release/bioc/html/DESeq2.html). Differential expressed genes were selected using highly expressed (threshold read number set as median of all expressing genes), and either a significantly changed (P value < 0.05) of 1.6 fold change (Figure 3A, B) or a 2-fold change (Figure 4A, B; Figure 5B, Figure 6A, E, F; Figure S4A, B) difference between at least two populations was chosen. Gene expression matrix (Heatmap differential clustering) was clustered using k-means algorithm (MATLAB function kmeans, MathWorks, https://www.mathworks.com/downloads/?requestedDomain=www.mathworks.com) with correlation as the distance metric. The value of k was chosen by assessing the average silhouette (MATLAB function silhouette) for a range of possible values (4-15).

Heatmaps graphics was performed with GeneE software (Broad Institute, https://software.broadinstitute.org/GENE-E/download.html).

qRT-PCR of miRNAs
In the case of sorted cells, 50-250 ng of total RNA isolated from microglia/ colon MFs/ Liver MFs (KCs) with miRNeasy micro-kit (QIAGEN) was reverse transcribed with the miScript reverse transcription kit (QIAGEN) according to the manufacturer's instructions, resulting in reverse transcription of both mRNA and miRNAs. The miScript SYBR Green kit (QIAGEN) was used to detect amplification in an Applied Biosystems 7300 Real-Time PCR machine, for specific miRNAs.

qRT-PCR of mRNAs
RNA was isolated by Ambion Dynabeads® mRNA DIRECT Kit. 10,000 - 30,000 microglia were sorted directly into the Lysis/Binding buffer supplied with the kit and isolation was performed according to the manufacturer's instructions. RNA was then reverse transcribed with the AffinityScript cDNA synthesis kit (Agilent Technologies). PCRs were performed with the SYBR green PCR Master Mix (Applied Biosystems) and the Applied Biosystems 7300 Real-Time PCR machine.

Genomic DNA isolation
10,000 - 30,000 microglia were sorted into LoBind eppendorff tubes (Sigma) containing RPMI supplemented with 10% FBS (Fetal bovine serum). Next, cells were centrifuged and pellet was either frozen or directly lysed for DNA isolation with Dneasy blood and tissue kit (QIAGEN). Dicer allele recombination in sorted microglia was analyzed with genotyping primers described in the section below - Genotyping Dicer floxed and recombined allele under methods details.

Genotyping Dicer floxed and recombined alleles
Routine genotyping of *cx3cr1^{Cre}:Dicer$^{fl/fl}$ and cx3cr1^{CreER}:Dicer$^{fl/-}$* mice was performed by PCR using following primers: *Dicer* WT/fl - FW (5′- ACAGTGACGGTCCAAAGTAAAG −3′), *Dicer* WT/fl - Rev (5′- CATGACTCTTCAACTCAAACT - 3′), *Dicer* recombined fl -Rev

(5′- CCTGAGTAAGGCAAGTCATTC −3′). These primers amplify a 350bp DNA fragment for the WT Dicer allele, 420 bp DNA fragment for floxed *Dicer* allele, and a 550 bp DNA fragment for the recombined *Dicer* allele.

Electrophysiology on brain slices (LTP)

Extracellular recordings in acute slices prepared from dorsal hippocampus were performed as previously described (Maggio and Segal, 2007). Following anesthesia with ketamine/xylazine (0.13/0.01 mg/g body weight), animals were rapidly decapitated, the brain removed, and 400 μm slices prepared using a vibroslicer. Slices were incubated for 1.5 hr in a humidified, carbonated (5% CO2 and 95% O2) gas atmosphere at 33 ± 1°C and perfused with artificial cerebrospinal fluid (ACSF) containing: 124mM NaCl, 2mM KCl, 26mM NaHCO3, 1.24mM KH2PO4, 2.5mM CaCl2, 2mM MgSO4, and 10mM glucose (pH 7.4) in a standard interface chamber. Recordings were made with a glass pipette containing 0.75M NaCl (4 MΩ) placed in stratum radiatum of CA1. Stimulation of Schaffer's collaterals was evoked using a pulse stimulator and delivered through a bipolar nichrome electrode. Input-output curves were run on each slice prior to beginning of each experiment. Before applying the tetanic stimulation, baseline values were recorded at a frequency of 0.033 Hz. LTP was induced by high-frequency stimulation (HFS) consisting of 100 pulses at twice the test intensity, delivered at a frequency of 100 Hz (1 s). Responses were digitized at 5 kHz and stored on a computer. Spike 2 software (Cambridge Electronic Design) was used for data acquisition.

Comet assay

The comet assay (Trevigen Inc., Gaithersburg, MD) was performed according to the manufacturer's protocol using neutral conditions. After lysis overnight at 4°C, the slides were washed twice with 1X Tris-borate EDTA buffer solution, pH 8.3 (TBE) for 10 min each. The slides were placed in a horizontal electrophoresis chamber and covered with TBE buffer. Electrophoresis was carried out at the rate of 1.0 V/cm for 20 min. The slides were removed from the electrophoresis chamber, washed in deionized water for 5 min and immersed in ice cold 100% ethanol for 5 min. Subsequently, the slides were air-dried, DNA was stained with 50 μL of SYBR Green I dye 1:10,000 in Tris–EDTA buffer, pH 7.5 for 20 min in the refrigerator and analyzed using an Olympus digital camera attached to an Olympus BX51 epifluorescence microscope.

Motoric activity assay

Home-cage locomotion. Mice were single-housed, and locomotive activity was examined automatically over a 48-h period using the InfraMot system (TSE Systems, GmbH).

Rotarod test. Mice were placed on an accelerating spinning wheel and their latency to fall was measured by an inframot beam. Mice were placed on a spinning wheel for five consecutive times, first two repetitions were considered training and last three repetitions were scored and averaged.

Hangwire test. Mice were attached to a wire by their forelimbs and their latency to grip wire with hind limbs was measured. Scoring equals the latency time, no grip or alternatively a fall was considered as "60 sec." Test was repeated 3 times with a 30 min gap between repetitions, scoring represented the average score of the three repetitions.

Bioinformatic prediction of miRNA target enrichment in a gene database

For measuring enrichment of miR targets in a gene data-set, a database of mouse miRNA predicted targets file was downloaded from TARGETscan7 (conserved miRNA families, all targets). Statistical significant enrichment of miRNA targets within the gene data-set of LPS treated Dicer deficient microglia upregulated genes, was calculated by two different statistical tests: a hypergeometric test using an in house developed script to count the mutual genes between the two data-sets as well as the size of each dataset and perform the statistical test with R (https://bbcunit.atlassian.net/wiki/display/BP/miR+target+enrichment+for+mouse) (see Supplemental Data 1) and a gene-set–enrichment-analysis (using the pre-ranked GSEA software, Broad Institute, as described (Subramanian et al., 2005)). For the GSEA software analysis the genes were pre-ranked by the RNA-Seq fold change and the enrichment was tested against the mouse miRNA targets. Differences were considered significant when $p < 0.05$.

Similarity measure between distinct lists of differentially expressed genes

For measuring similarity of differentially expressed genes in Dicer deficient whole brain microglia and hippocampal microglia in response to LPS (see Figure 5A), a Pearson correlation test was applied, using Partek software.

QUANTIFICATION AND STATISTICAL ANALYSIS

The statistical details of experiments can be found at the figure legends section. Data are displayed as individual dots and mean, except for Figure 7D, S1E, S6C and S7C and D, where the data are presented as bar graph with mean ± SEM.

"N" represents the number of individual mice used in the experiment, except for Figure 1A, where N represents number of samples, and each sample is a pool collected from 6 WT mice. Of note, sizes of the tested animal groups were also dictated by availability of the transgenic strains and litter sizes, allowing littermate controls. Pre-established exclusion criteria are based on IACUC guidelines. Animals of the same age, sex and genetic background were randomly assigned to treatment groups. The investigator was not blinded to the mouse group allocation. Tested samples were blindly assayed.

Statistical analysis for differences between two or more groups was performed using GraphPad Prism (GraphPad Software, Version 6.0, La Jolla, USA). All data were tested for normality applying the Kolmogorov-Smirnov test. If normality was given, an unpaired t test was applied in the case of two groups comparison. In the case of more then two groups comparison, a one-way Anova was performed followed by an unpaired t test for multiple comparisons. Statistical significance was defined as $p < 0.05$.

Bioinformatic data analysis

RNA seq (MARS-Seq) and miRNA microarray data analysis is described in the Method details section, under RNA-seq, Processing and Analysis and Agilent microRNA microarray, respectively.

DATA AND SOFTWARE AVAILABILITY

The accession numbers for datasets reported in this paper are GEO (GSE98144): including GSE98143 (Agilent chip), and GSE98142 (RNA-seq).

Guidelines for the R script used to measure enrichment of miR targets in a gene data-set (https://bbcunit.atlassian.net/wiki/display/BP/miR+target+enrichment+for+mouse) (see Key resource Table and method details section under Bioinformatic prediction of miRNA target enrichment in a gene database), is provided as supplemental text (see Data S1).